The Greenhouse Gas Climate Commitment and Reversibility of Peak Warming from Past Emissions

Alexander J. MacIsaac

A Thesis

In

The Department of

Geography, Planning and Environment

Presented in Partial Fulfillment of the Requirements

For the Degree of Master of Science (Geography, Urban and Environmental Studies) at

Concordia University

Montreal, Quebec, Canada

August 15, 2019

© Alexander J. MacIsaac

CONCORDIA UNIVERSITY

School of Graduate Studies

This is to certify that the thesis prepared

By: Alexander J. MacIsaac

Entitled: The greenhouse gas climate commitment and reversibility of peak warming from historic emissions

and submitted in partial fulfillment of the requirements for the degree of

Master of science (Geography, Urban and Environmental Studies)

complies with the regulations of the University and meets the accepted standards with respect to originality and quality.

Signed by the final Examination Committee:

_____ Chair
Dr. Jeannine St-Jacques

_____ Internal Examiner
Dr. Nadine Mengis

_____ External Examiner
Dr. Andrew MacDougall

_____ Supervisor
Dr. H. Damon Matthews

Approved by _____
Dr. Pascale Biron
Chair of Department

_____
Dr. André Roy
Dean of Faculty of Arts and Science

Date _____

ABSTRACT

The greenhouse gas climate commitment and reversibility of peak warming from historic emissions

The warming caused by past CO_2 emissions is known to persist for centuries to millennia, even in the absence of additional future emissions. Other non-CO_2 greenhouse gas emission have caused additional historical warming, though the persistence of this non-CO2 warming varies among gases owing to their different atmospheric lifetimes. Under deep mitigation scenarios or in an idealized scenario of zero future greenhouse gas emissions, the past warming from shorter-lived non-CO_2 gases has been shown to be considerably more reversible than that caused by CO_2 emissions. Here I use an intermediate-complexity global climate model coupled to an atmospheric chemistry module to quantify the warming commitment and its reversibility for individual and mixtures of non-CO2 greenhouse gases. I show that warming caused by gases with short atmospheric lifetimes will decrease by more than half its peak value within 30 years following zeroed emissions at present day, with more 80 percent of peak temperature reversed by the end of this century. Despite the fast response of atmospheric temperature to the elimination of non-CO_2 emissions, the ocean responds much more slowly: past ocean warming does not reverse, but rather continues for several centuries after zero emissions. Further consequences are shown for the land carbon pool, which decreases as an approximately linear function of historical non-CO_2 greenhouse gas induced warming. Given that CO_2 and non-CO_2 greenhouse gas emissions share common emission sources, I also explore a set of scenarios where sets of emissions are zeroed according to two broad source categories: (1) fossil fuel combustion, and (2) land-use and agriculture. Using these additional model runs, I investigate the temperature change that is avoided if all CO_2 and non-CO2 greenhouse gas emissions from a particular source abruptly stops while

others are allowed to continue. These results indicate the possibility of land-use change and agriculture activities continuing under deep mitigation scenarios and ambitious climate targets, without leading to exceedance of global climate targets. Though I analyze unlikely scenarios, my work provides baselines from which more realistic mitigation scenarios can be assessed. The reversibility of peak temperature caused by historic non-CO_2 gases is a relevant measure for policy frameworks seeking to limit global warming to ambitious targets, such as the 1.5 ^{o}C target adopted by the Paris Agreement

ACKNOWLEDGEMENTS

First and foremost, I would like to thank and acknowledge the generous support of my supervisor, Professor Damon Matthews. Without his teaching and guidance this work would not have been possible. Professor Matthews's knowledge and tact has served as a constant and continued inspiration throughout the development of this work.

I am greatly indebted to the support of Dr. Nadine Mengis, who lead me through the practice of climate modelling and who helped steer my research approach. Thank you for keeping me on track and for regularly helping me to navigate the processes of climate modelling.

I would like to thank my fellow lab mates and colleagues, particularly: Antii-IlariPartanen, who helped conceive the modelling approach used here; Dony Seto and Etienne Guertin, who assisted with modelling set up and helping to solve modelling errors; Maida Hadziomanovic, who helped review my initial research questions; and Nesha Wright, from Simon Fraser University, who worked with Dr. Mengis on additional updates to the climate model used here.

In addition, I would like thank my partner, roommates, and parents for their dedicated support and willingness to help me succeed.

Finally, it is with a heavy heart that I would like to dedicate this work to my late friend Tyler Anthony Kays, who saw first that I wanted be an Environmental Scientist and whose friendship I deeply miss.

CONTRIBUTION OF AUTHORS

MANUSCRIPT (TO BE SUBMITTED)

H. Damon Matthews	Research supervisor, funding, writing and editing, calculations development (particularly Eq. 5.1), and data analysis

TABLE OF CONTENTS

List of Figures ix

List of Tables x

List of Abbreviations xi

Glossary xii

CHAPTER 1: Introduction 1

1.1 The historical climate commitment 1

1.1.1 Non-CO_2 greenhouse gases and the climate system 2

1.1.2 The importance of emissions source 4

1.2 Research techniques and objects, and thesis structure 4

CHAPTER 2: Literature Review 6

2.1 Climate response to cumulative CO_2 emissions 6

2.2 Human influence, non-CO_2 GHGs, and emissions classification methods 9

2.3 Zero emissions commitments and the climate system 13

2.4 The importance of non-CO_2 GHGs 19

CHAPTER 3: Research Questions 22

2.5 Research questions 22

CHAPTER 4: Methods 23

4.1 UVic-ESCM 23

4.2 Atmospheric chemistry module 23

4.3 Atmospheric chemistry module validation 29

4.4 Land use change and agriculture 29

CHAPTER 5: Manuscript 31

5.1 Introduction 31

5.2 Model & simulations 33

5.2.1 Model 34

5.2.2 Simulations 35

5.2.3 Calculations.....37

5.3 Results 38

5.3.1 Historical and zero emissions temperature commitment 38

5.3.2 Peak temperature reversibility 42

5.3.3 Historical and long-term ocean temperature and carbon cycle changes 46

5.3.4 Fossil fuel and land use change 49

5.4 Discussion 52

5.5 Conclusion 57

CHAPTER 6: Expanded discussion and conclusion 59

6.1 Climate system response variability 59

6.2 Conclusions 61

References 65

LIST OF FIGURES

Figure 5.1: Historic and projected effective radiative forcing of non-CO_2 GHGs

Figure 5.2: Change in SAT relative to 1850 per simulation

Figure 5.3: Change in SAT relative to 1850 per simulation relative to CO_2

Figure 5.4: Peak and future SAT relative to 1850 per simulation

Figure 5.5: Future SAT relative to 2019 per simulation

Figure 5.6: Carbon & heat fluxes per simulation relative to CO_2

Figure 5.7: Carbon pools per simulation and per simulation relative to CO_2

Figure 5.8: Historic temperature vs land carbon pool per simulation relative to CO_2

Figure 5.9: FFC and LUC GHG concentration

Figure 5.10: FFC and LUC change in SAT relative to 1850

Figure 6.1: Sea-ice area-surface albedo feedback and variability

LIST OF TABLES

Table 4.1: GHG emissions in this study

Table 4.2: non-CO_2 GHG parameters

Table 4.3: Tropospheric-ozone parameters

Table 5.1: Non-CO_2 GHG emissions source partitions

Table 5.2: Average change in SAT per gas per late 20th century decade

Table 5.3: Percent of peak temperature remaining per simulation relative to CO_2

Table 5.4: FFC and LUC temperature change avoided

LIST OF ABBREVIATIONS

CFCs	Chlorofluorocarbons
CF_4	Tetrafluoromethane
CH_4	Methane
CMIP6	Coupled Model Intercomparison Project phase 6
CO	Carbon monoxide
CO_2	Carbon dioxide
ERF	Effective radiative forcing
F-gases	Fluorinated gases
FAIR 1.3	Finite Amplitude Impulse Response model, version 1.3
FFC	Fossil Fuel Combustion
GHG	Greenhouse gas
HCFCs	Halo-chlorofluorocarbons
HFC	Fluorocarbons
LUC	Land-use change and agriculture
N_2O	Nitrous oxide
NMVOC	Non-methane volatile organiccarbons
NO_x	Nitrogen oxides
ODS	Ozone depleting substances
OH	Hydroxyl radicle
RCP	Representative concentration pathway
SAT	Global average surface air temperature
SLCFs	Short-lived climate forcers
SLCPs	Short-lived climate pollutants
SST	Global average sea surface temperature
TCRE	Transientclimateresponse to cumulative carbondioxideemissions
Trop-ozone	Tropospheric ozone
UVic-ESCM	University of Victoria Earth Systems Climate Model
ZEC	Zero emissions commitment

GLOSSARY

Zero Emissions Commitment	A climate modelling scenario with forcing from historical emissions, or a proxy thereof, that abruptly stop in a given year.
Climate commitment	The general term used to refer to the impact of historical anthropogenic emissions on the climate system in the absence of future emission. Used here to indicate either an increase or decrease in temperature change following zeroed emissions
Warming commitment	Positive temperature change following zeroed emissions
Warming reversibility	Negative temperature change following zeroed emissions
Temperature commitment	The climate commitment specific to atmospheric temperature change
Peak warming/temperature change	The maximum temperature change in a given simulation

CHAPTER 1
INTRODUCTION

1.1 The historical climate commitment

Under the Paris Agreement, nations will attempt to keep global temperature from exceeding 1.5 °C above pre-industrial levels (UNFCC, 2015). This is an ambitious target, and will require detailed knowledge about how climate will respond to all drivers of temperature change. Extensive research has shown the main driver of long-term temperature change is cumulative carbon dioxide (CO_2) emissions (Allen et al., 2009; Matthews et al., 2009; Matthews & Solomon, 2013;Gillett et al., 2013; Tokarska et al., 2016; Matthews et al., 2018). This is the most important anthropogenic greenhouse gas (GHG), and persists in the atmosphere on timescales of a century to multiple-millennia (Eby et al., 2009; Ciais et al., 2013; Solomon et al., 2009; Matthews & Zickfeld, 2012; Zickfeld et al., 2012; Frolicher et al., 2014; Frolicher & Paynter, 2015; Ehlert & Zickfeld, 2017; Mauritsent & Pincus, 2017; Williams et al., 2017; Smith et al., 2019). Short of actively removing it from the atmosphere (Tokarska & Zickfeld, 2016; Zickfeld et al., 2016), the CO_2 burden from past and current CO_2 emissions commits global temperatures to remain approximately stable, even in the absence of additional emissions (Solomon et al., 2009; Matthews & Zickfeld, 2012; Frolicher et al., 2014; Frolicher & Paynter, 2015; Ehlert & Zickfeld, 2017; Mauritsent & Pincus, 2017; Williams et al., 2017; Smith et al., 2019). In other words, warming caused CO_2 emissions is effectively irreversible on human timescales (Matthews & Solomon, 2013).

According to the Global Warming Index (Haustein et al., 2017), current temperature change is near 1.1 °C above the pre-industrial baseline. As a result of the influence of historical

CO_2 emissions on the carbon cycle, the climate system is committed to much of this current global warming, and associated impacts, for the foreseeable future (Matthews & Zickfeld, 2012; Matthews & Solomon, 2013). In contrast, the current warming caused by historical non-CO_2 greenhouse gases with shorter atmospheric lifetimes can be reversed over long timescales with ambitious mitigation efforts (Bowerman et al., 2013; Zickfeld et al., 2017). These climate commitments – warming, stable, or cooling – have been estimated using the conceptual scenario of "Zero Emissions Commitment" (ZEC), which defines the change in temperature caused by past emissions, at a given point in the future after emissions have been set to zero (Solomon et al., 2009; Matthews & Zickfeld, 2012; Allen et al., 2018b).

1.1.1 Non-CO_2 greenhouse gases and the climate system

For past emissions from CO_2, results from ZEC simulations depend on how historical changes to the carbon cycle evolve in the absence of additional forcing and on ocean thermal inertia (Solomon et al., 2009; Ehlert & Zickfeld, 2017). For past emissions from non-CO_2 greenhouse gases and aerosols, results from ZEC simulations depend on the rate of atmospheric concentration decline in the absence of additional emissions and on the effective radiative forcing of individual gases (Matthews & Zickfeld, 2012; Zickfeld et al., 2017; Allen et al., 2018b).Though not analyzed here, the effect on future temperature from past emissions of aerosols is different from that of greenhouse gases because in the absence of aerosol emissions temperature rises, for a magnitude and duration dependent on the additional forcing that continues in the future (Matthews & Zickfeld, 2012; Allen et al., 2018b).

Because the rate of atmospheric concentration decline of non-CO_2 GHGs following zero emissions is a driver of temperature decline (Matthews & Zickfeld, 2012; Bowerman et al., 2013;

Zickfeld et al., 2017; Allen et al., 2018b), historical warming induced by emissions from those gases is thought to be partly reversible. This means that if non-CO_2 greenhouse gas emissions are allowed to continue, a portion of the global warming those emissions induce up to the point of deep mitigation, or zero emissions, will reverse itself in the absence of additional forcing (Bowerman et al., 2013; Zickfeld et al., 2017; Collins et al., 2018). There is therefore a need to quantify that portion of warming reversibility: my study fills this gap by assessing the reversibility of peak warming induced by historical non-CO_2 GHG emissions. To account for the wide range of atmospheric lifetimes and radiative efficiencies of non-CO_2 greenhouse gases (Myhre et al., 2013; Smith et al., 2018), I analyze the reversibility of peak temperature changes over decadal and centennial timescales. To better understand the influence of individual and select mixtures of past non-CO_2 GHG emissions on the future climate commitment, I here disaggregate non-CO_2 GHG emissions into policy-relevant groupings. These are: methane (CH_4), nitrous oxide (N_2O), CH_4& N_2O together, fluorinated gases (F-gases or Kyoto Protocol gases), ozone depleting substances (ODS or Montreal Protocol gases), and tropospheric-ozone (trop-ozone) (Myhre et al., 2013).

By means of individual processes that are not directly involved with the carbon cycle, additional historical warming caused by non-CO_2 GHGs emissions can further cause decreases in the land (soil and biosphere) and ocean carbon pool, with increases in the atmosphere carbon pool (MacDougall & Knutti, 2016; Collins et al., 2018). Decreases in the land carbon pools occur because additional warming causes increased decomposition of soil organic matter and increased plant respiration (processes that release carbon into the atmosphere) (MacDougall & Knutti, 2016; Collins et al., 2018). Decreases in the ocean carbon pool occur because the rate of ocean carbon dissolution slows with increasing sea-surface temperature, which increases with atmospheric warming (MacDougall & Knutti, 2016; Zickfeld et al., 2017). Here I disaggregate this influence

per individual and non-CO_2 GHG groupings and examine the relationship between additional temperature change increase and decreases in the land carbon pool.

1.1.2 The importance of emissions source

Though my analyses focus on policy relevant groupings of non-CO_2 gases, the sources of emissions are another important method by which to evaluate future temperature change. Two general sources of human emissions are fossil fuel combustion (FFC) and land-use change/agriculture (LUC), which both produce a mixture of greenhouse gases and aerosols (Ciais et al., 2013; Mengis & Matthews, 2019). The combination of gases emitted by each source can be partitioned into the percentage of individual gas emissions resultant from either FFC or LUC activities (Mengis & Matthews, 2019). In this study, I use these partitions to analyse how temperature changes in the absence of one activity (e.g. LUC, including agriculture), while continuing emissions from all other activities (e.g. FFC and other anthropogenic activities), and vice versa.

1.2 Research techniques and objectives, and thesis structure

To simulate the climate effect of non-CO_2 GHG emissions changes, I built a simple atmospheric chemistry module (see Chapter 3.2) within the University of Victoria Earth Systems climate model (UVic-ESCM), a climate model of intermediate complexity (Weaver et al., 2001). I used ZEC simulations to quantify the reversibility of peak temperature and to analyze the effect of historical non-CO_2 GHG emissions on simulated carbon pools. The subsequent analysis of by-source future temperature change was done with a variation on the ZEC method, where I zeroed emissions in one sector while allowing emissions in all other sectors to continue.

In using ZEC scenarios, where GHG emissions are assumed to stop at the present-day, my work should be viewed as highly idealized. This work, however, is relevant because it 1) provides baselines of future temperature change caused by individual greenhouse gases, 2) defines timeline for the natural reversibility of peak temperature changes caused by past GHG emissions, 3) defines the effect of non-CO_2 GHG warming on the land and ocean carbon pools, and 4) provides a measure by which continued human activities by sector could influence temperature change.

The following sections of this thesis include a literature review (Chapter 2), modelling considerations (Chapter 3), a manuscript (Chapter 4), and an expanded discussion and conclusion (Chapter 5).

CHAPTER 2
LITERATURE REVIEW

2.1 Climate response to cumulative CO_2 emissions

The climate system is a dynamic network of physical, chemical and energy processes evolving over timescales of days to millennia, and involving interactions between the hydrosphere, lithosphere, biosphere, atmosphere, and cryosphere (Baede et al., 2001). These processes include, but are not limited to: precipitation, pressure (wind), temperature, photosynthesis, weathering, and movement of energy or heat (radiative forcing) (Baede et al., 2001). Changes in the system are driven by both natural and human perturbations to the planetary energy budget (Myhre et al., 2013). Energy to the system is forced externally by solar output, orbital variation, and volcanic activity (Baede et al., 2001; Myhre et al., 2013). In principle, radiative energy is supplied daily by solar output that is either reflected back to space or absorbed by water, land surfaces, and the atmosphere (Baede et al., 2001). At night land surfaces re-emit radiative energy which either escapes to space or is trapped by GHGs in the atmosphere that are themselves radiative forcers on the climate system (Baede et al., 2001).

This radiative energy in the climate system is otherwise called heat and though its only source is solar output, radiative energy flows between and is stored in the internal climate system components (Baede et al., 2001). Considering the planetary land surface as a uniform body, sustained increase in radiative energy translates into temperature increase at the surface by a simple relationship whereby temperature change is proportional to radiative forcing and climate sensitivity (Myhre et al., 2013).

Owing to the significant difference in heat capacity between the land and the ocean, the ocean can absorb far greater quantities of radiative energy than the land (Baede et al., 2001). As such, the ocean both does not re-emit radiative energy to the same degree as land surfaces, and it is the driver of the thermal inertia of the climate system (Baede et al., 2001). This means that with any change to the radiative balance of the system, there is a lagged effect on the temperature of the ocean and as a consequence on global temperatures (Hansen et al., 2005; Ricke & Caldiera, 2014; Zickfeld & Herrington, 2015). While the ocean can uptake energy from the atmosphere, the capacity to do so decreases as temperate increases (Solomon et al., 2009; Ehlert & Zickfeld, 2017).

If we look at the climate system as it exists today, such changes to the radiative balance can be measured by changes to the internal cycles of the climate system. Internal changes to vegetation, land surface, sea and land ice, ocean, and atmospheric processes all affect the system. Research has shown the most dominant forcers on internal components are that movement of energy between the atmosphere and ocean (and associated feedbacks from the other components) and the carbon cycle (Myhre et al., 2013; Ehlert & Zickfeld, 2017).

Affected by temperature changes, as well as its own internal and external processes, the carbon cycle is the movement of carbon (organic, inorganic, dissolved inorganic, and CO_2) between the components of the climate system (Ciais et al., 2013). Because CO_2 is a greenhouse gas (gases that trap and re-radiate radiative energy), changes in the atmospheric concentration of CO_2 lead to changes in the radiative balance of the climate system and thus translate into changes in surface air temperature (SAT) and sea-surface temperature (SST) (Baede et al., 2001). Natural processes of plant and animal respiration, and tectonic outgassing lead to increases in the atmospheric concentration of CO_2, while photosynthesis, ocean dissolution, and silicate weathering lead to decreases in atmospheric CO_2 (Ciais et al., 2013), and associated increases in

the land (biosphere and soil) and ocean carbon pools. These sinks function on yearly, centennial, and multiple-millennia timescales and the balance of natural input and output can be disturbed by emitting CO_2 into the atmosphere and increasing SAT and SST (Ciais et al., 2013).

For example, human output of CO_2 beyond the efficacy of the short-term sinks causes a portion the emissions to accumulate in the atmosphere (Ciais et al., 2013).Climate modelling research has shown cumulative CO_2 emissions and SAT change are approximately linearly related (Allen et al., 2009; Matthews et al., 2009; Gillet et al., 2013; Tokarska et al., 2016; Matthews et al., 2018). Called the transient climate response to cumulative carbon dioxide emission (TCRE), this response emerges as a combination of the non-linear processes of CO_2 radiative forcing and removal from the atmosphere by sinks (Matthews et al., 2009; Gillet et al., 2013; MacDougall & Friedlingstein, 2015). As cumulative emissions increase, increasing SAT decreases the efficacy of biosphere sinks and increasing SST decreases the efficacy of ocean carbon dissolution, leading to a larger airborne fraction of emissions (MacDougall et al., 2015). However, this larger fraction exhibits a smaller per-unit radiative forcing due to saturation of absorption bands (MacDougall et al., 2015). Therefore, each unit of CO_2 emissions induces approximately the same climate response.

Calculations of the TCRE yield a range of values but a recent assessment of the literature in this field by Matthews et al. (2018), placed a best estimate for the TCRE at 1.6 ºC per trillion tonnes of cumulative CO_2 emissions, within the range of 0.8 to 2.4 ºC per $TtCO_2$. Constraining these results by observations of temperature increase versus CO_2 emissions yielded a TCRE of 1.35 ºC per $TtCO_2$, with a range of 0.7 to 2.0 ºC per $TtCO_2$(Matthews et al., 2018).A strong advantage of the TCRE is that inverting it yields the amount of cumulative CO_2 emissions that would be responsible for a given temperature change (Matthews et al., 2009; Zickfeld et al., 2009;

Collins et al., 2013; Rogelj et al., 2013; Millar et al., 2016; Matthews et al., 2017; Millar et al., 2017).

This is the basis of a carbon budget – the amount of CO_2emittable before a specific temperature threshold is breached. For the ambitious temperature threshold set by the Paris agreement of 1.5 ^{o}C (UNFCCC, 2015), the TCRE concept has been used to define both the total carbon budget (from a pre-industrial baseline to the temperature threshold) and the remaining carbon budget after accounting for past cumulative CO_2 emissions. From a recent estimate accounting for historical cumulative CO_2 emissions up to 2018, the remaining carbon budget has been calculated at 580 $GtCO_2$ (Allen et al., 2018b). Though attractive in terms of policy approaches (Millar et al., 2017), a caveat to the concept of carbon budgets is that they apply to cumulative CO_2 emissions and cannot, by measure of the TCRE, be directly related to the historical or future warming caused by non-CO_2 GHGs. Most analyses therefore adjust downwards the total or remaining carbon budget as a function of warming from non-CO_2 gases additional to the warming from CO_2 (Frame et al., 2014; MacDougall et al., 2015; Millar et al., 2016; Matthews et al., 2017; Collins et al., 2018).

2.2 Human influence, non-CO_2 GHGs, and emissions classification methods

Given the natural variability of the climate system, human influenced changes in the system are driven by perturbations to the chemical structure of the atmosphere that either lead to positive or negative radiative forcing, or both, and by changes to the land surface (Myhre et al., 2013). Causes of human influence on the climate system result from activities which increase the concentrations of GHGs and other pollutants in the atmosphere and which alter the solar reflectivity of land surfaces (Baede et al., 2001; Myhre et al., 2013). By burning fossil fuels,

growing agricultural crops, building cities and cutting forests, and refrigerating produce, humans emit both gases and particulate matter into the atmosphere (Myhre et al., 2013). These pollutants are emitted or co-emitted from individual or multiple sources and persist in the atmosphere for days to multiple-millennia depending on the type of pollutant (Ciais et al., 2013; MacDougall & Knutti et al., 2016; Saunois et al., 2016; Le Quere et al., 2018). Due to the positive or negative effect on radiative fluxes, the combination of sources, and wide range of persistence of emissions, human influence on the climate system is a challenge to quantify.

Although the TCRE explains the relationship between cumulative CO_2 emissions and temperature change, it does not, as is, apply to changes in radiative forcing driven by non-CO_2 GHGs. One difference in quantifying the climate response from CO_2 and non-CO_2 GHGs is that each non-CO_2 GHG (see Tables3.1 &3.2 for a listing of gases included here) exhibits its own effective radiative forcing (ERF) dependent on the radiative efficiency of the gas and the concentration of the gas relative to pre-industrial levels (Myhre et al., 2013; Smith et al., 2018).

The change in concentration of each non-CO_2 gas is further a function of their natural sinks. Many non-CO_2 GHGs (including those listed in Tables 3.1 &3.2), are chemically reactive in the atmosphere and their atmospheric sink is a process of chemical reactions involving the hydroxyl radical (OH^-) (Levy, 1979; Seinfeld & Pandis, 2016). Within this atmospheric chemistry, non-CO_2 GHGs have their own cycles that are less affected by changes in temperature or the carbon cycle than CO_2. One part of the atmospheric chemistry cycles is the decay rate of non-CO_2 GHG concentrations. Non-CO_2 GHGs span a range of atmospheric lifetimes from days (e.g. tropospheric ozone) to multiple-millennia (e.g. CF_4) (see Table 3.2) (Smith et al., 2012; Myhre et al., 2013; Smith et al., 2018). Gases with atmospheric lifetimes at the lower end of this range do not remain in the atmosphere under deep mitigation and are hence short-lived (Smith et al., 2012; Bowerman

et al., 2013; Myhre et al., 2013). These differences in ERF and atmospheric chemistry cycles (including, for some gases, natural perturbations) effectively means the radiative forcing from non-CO_2 GHGs is separate from CO_2.

With respect to non-CO_2 gases and considering their individual differences in radiative efficiency and atmospheric lifetime, a challenge for aggregating the radiative forcing from non-CO_2 GHGs is the choice of substance classification method. How substances are grouped together will impact which properties of the emissions are aggregated and therefore obfuscated. For example, substances exhibiting atmospheric lifetimes on decadal timescales or less have been termed short-lived climate forcers (SLCFs) or short-lived climate pollutants (SLCPs) (Shindell et al., 2012; Smith et al., 2012; Pierrehumbert, 2014;Rogelj et al., 2014; Allen et al., 2016). SLCFs and SLCPs include both positive radiative forcers (non-CO_2 GHGs) and net negative forcers (aerosols) (Pierrehumbert, 2014; Rogelj et al., 2014).In using atmospheric lifetime as the amalgamating parameter, the individual radiative efficiency and concentration nof each pollutant is more hidden. This means the effect of a GHG with a low effective radiative forcing, such as flouro-carbons (HFCs), chlorofluorocarbons (CFCs), halo-chlorofluorocarbons (HCFCs), and halocarbons, will be obscured by the effect of a GHG with a larger forcing, such as methane (CH_4). A wider range grouping is the non-CO_2 climate forcers, which includes all anthropogenic climate forcers other than CO_2 and including land-use change (an activity that both causes emissions and influences radiative forcing) (Myhre et al., 2013; Matthews et al., 2017). Under a non-CO_2 climate forcers classification, aggregation includes both atmospheric lifetime and radiative efficiency, thus further masking the effect from any one forcer.

Policy frameworks offer a different approach to classifying anthropogenic emissions. The Montreal Protocol banned the use of chlorofluorocarbons and similar substances from refrigerants

because they were shown be causing a hole in the stratospheric ozone layer (UNEP, 1987). Though these ozone depleting substances (ODSs) exhibit yearly to millennia lifetimes, they do show similar radiative efficiencies, are within an order of magnitude of the same atmospheric concentration (at present), and are almost all only emitted anthropogenically. As an extension on the Montreal Protocol, the Kyoto Protocol grouped the fluorinated gases (F-gases), setting objectives to limit their emissions (UNFCCC, 1998). Because F-gases include multiple compounds with millennia scale atmospheric lifetimes, using this group limits the capacity to capture changes on centennial or less scales. However, by following policy formed classifications, as I do here, conclusions more directly impact policy decisions and more closely follow emissions scenarios developed in relation to international agreements (van Vuuren et al., 2011; Riahi et al., 2017).

A third classification method, and secondary method used here, for human influenced radiative forcing is by source. As noted above ODSs are grouped by their common effect on the atmosphere but they also share a common main source: refrigerants. The remaining high level sources are fossil fuel combustion (FFC) and land-use change / agriculture (LUC) (Ciais et al., 2013; Myhre et al., 2013). All other sources, including refrigerants, can additionally be grouped as other anthropogenic activities. Emissions from fossil fuels result from burning carbon-based fuels for energy. The primary resulting pollutant is CO_2, but the production and use of fossil fuels also produces methane (CH_4), nitrous oxide (N_2O), tropospheric ozone precursors (trop-ozone), and minor F-gases output as co-emissions (Baede et al., 2001; Ehalt et al., 2001;Ciais et al., 2013; Myhre et al., 2013). Land-use change involves any activity that changes the landscape, including agriculture as well as biomass burning. With agriculture, N_2O (from the use of nitrogen fertilizers) and CH_4 (from livestock and rice production) are co-emitted along with or independently from

CO_2, where agriculture is the larger source of CH_4 and N_2O gases compared to fossil fuel combustion (Baede et al., 2001; Mengis & Matthews, 2019).

2.3 Zero emissions commitments and the climate system

Regardless of the chosen classification method, non-CO_2 GHGs are known to influence radiative forcing and therefore constitute an additional challenge in quantifying the current and future human impact on the climate system. With historical data, climate forcing from past and current emissions can be used to render a snapshot of the climate system and warming experienced today (Haustein et al., 2017; Mauritsen & Pincus, 2017; Allen et al., 2018b). Projecting climate change into the future is done through a variety of methods and emissions projects and, due to our inability to predict human actions over long periods, is generally very uncertain. The level of climate change today from past emissions, however, can be shown to extend multiple centuries into the future through zero emissions commitment scenarios (ZEC) (Matthews & Zickfeld, 2012; Allen et al., 2018b).

ZEC scenarios are a method used to understand how climate will continue to change (i.e. continue warming, or cool over time) in response to the emissions that are already in the atmosphere (Solomon et al., 2009; Matthew & Zickfeld, 2012; Ehlert & Zickfeld, 2017; Mauritsen & Pincus, 2017). These scenarios are constructed by driving a global climate model with historical anthropogenic forcing (or a proxy to it), then setting emissions to zero and observing changes over the proceeding centuries or millennia, termed here the climate commitment, it is calculated by assessing the change in atmospheric temperature from the time emissions were zeroed to the end of the simulation. This commitment has been called the warming commitment for results that are

greater than zero (Ehlert & Zickfeld, 2017)[1], but results less than zero could be termed the warming reversibility – i.e. the amount of temperature change that is reduced due to emissions stoppage over a given period of time.

As a function of past emissions, the long-term climate commitment is dominantly dependent on historical cumulative CO_2 emissions (Matthews & Zickfeld, 2012). However, the climate commitment is additionally dependent on historical non-CO_2 forcing, the climate system parameters considered (i.e. which climate model is used to simulate the response), the proximity of the system equilibrium, which types of emissions are zeroed, and the length of ZEC simulation (Solomon et al., 2009; Matthew & Zickfeld, 2012; Ehlert & Zickfeld, 2017,Zickfeld et al., 2017; Allen et al., 2018b). One early benefit of CO_2-only ZEC scenarios is that they can capture climate inertia (dominated by the ocean response) and with it can be used to estimate the maximum (or peak) temperature reached as a result of past emissions (Solomon et al., 2009; Matthew &Zickfeld, 2012; Ehlert & Zickfeld, 2017). Though highly idealized, ZEC scenarios are important measures of the current status of climate change, a strong approach for projecting and determining climate system baselines, and a simple metric against which to benchmark the effectiveness of mitigation strategies.

Under ZEC scenarios forced by lower quantities of CO_2-only, the temperature change resultant from past emissions remains approximately constant for multiple centuries (Solomon et al., 2009; Ehlert & Zickfeld, 2017). This constant temperature is the result of a balance between the efficacy of carbon sinks and the capacity of the ocean to uptake heat from the atmosphere (Ehlert & Zickfeld, 2017). After emissions cease CO_2 is initially removed from the atmosphere by

[1]The term "warming commitment" has also been applied to other climate commitment methodologies, such as the constant composition commitment and has been used to classify both positive or negative temperature changes (e.g. Zickfeld et al., 2013). Here, however, I use different terms to distinguish between a positive or negative temperature change and apply the terms climate commitment or temperature change when referring to either or.

a fast response from land sinks through photosynthesis as well as through as slow response from ocean dissolution. This process of CO_2 removal (or uptake) causes a decline in atmospheric CO_2 concentration, which by itself would cause surface temperatures to decrease (Ehlert & Zickfeld, 2017). At the same time, the ocean continues to take up radiative forcing (heat) from the atmosphere, storing it as a temperature change in the deep ocean via convection processes (Ehlert & Zickfeld, 2017, Zickfeld et al., 2017). Initially following zeroed emissions, the ocean will take up heat a higher rate but as this rate declines, less heat is taken out of the atmosphere (Ehlert & Zickfeld, 2017). This balance of declining CO_2 in the atmosphere, combined with a declining rate of ocean heat uptake, leads to approximately constant atmospheric temperatures for at least several centuries (Solomon et al., 2009; Ehlert & Zickfeld, 2017).

Despite the nearly constant atmospheric temperature following zero CO_2 emissions, the climatological effects of those emissions persist in other components of the system. Ocean heat uptake, for example, does not stop with CO_2 emissions: rather, the ocean continues to take up heat from the atmosphere for many centuries following ZEC, albeit at a reduced rate over time (Matthews & Zickfeld, 2013; Frolicher et al., 2014, Zickfeld et al., 2017). Because thermal sea-level rise results from thermal expansion of the ocean, which is driven by increases in ocean heat, sea-level rise will also continue for many centuries after CO_2 emissions cease (Solomon et al., 2009; Matthew & Zickfeld, 2012; Ehlert & Zickfeld, 2017; Zickfeld et al., 2017). At the time of stopping CO_2 emissions, the level of ocean temperature change is determined by the level of atmospheric temperature change, which is related to the cumulative CO_2 emissions (Matthews et al., 2012). Therefore, by an association to atmospheric temperature change, ocean temperature change and with it thermal sea-level rise are dependent on the cumulative CO_2 emissions prior to

zero emissions, and can be augmented by additional warming from non-CO_2 forcers before emissions stop.

At a simple understanding, responses in the climate system to external forcing can be induced by setting a given quantity of emissions from a forcer to a one-off pulse, then observing how the system reacts. Such emission pulse scenarios do not align exactly with ZEC scenarios, but they do offer a means to investigate the fast and slow responses of the climate system in a manner that is similar to the response from a ZEC scenario. Using an 1800 GtC pulse (representative of CO_2), Frolicher et al. (2014) calculated climate commitments from three different models yielding temperature change ranging from -0.06 to 0.37 °C following the emissions pulse. In a CO_2 pulse experiment driving temperature to 2 °C, Williams et al. (2017), found that after 600 years of zeroed emissions, temperature increases by approximately 0.6 °C. For these experiments, all three models used were Earth System Models with high resolution ocean structures, enabling observations of the geographic structure of ocean heat uptake. Between the poles, ocean heat uptake was shown to have higher rates in high latitudes and lower rate in low latitudes, meaning there is an exacerbated regional structure to ocean heat change (Frolicher et al., 2014).

This result has consequences when considering how of high levels of warming before zeroed emissions drive changes in the climate system. Higher levels of global warming are known to influence the poles greater than the tropics (Partenen et al., 2016), meaning under high warming scenarios the ocean should have a reduced potential to uptake carbon and possibly heat. Both Frolicher & Paynter (2015) and Ehlert & Zickfeld (2017) examined this impact using an idealized scenario where CO_2 concentration is increased by 1% per year until 2 °C temperature change was reached or until concentration was doubled, respectively. In Frolicher & Paynter's 2 °C analysis, the rate of ocean heat uptake was shown to decline faster than the decline in heat uptake from land

and ocean CO_2 uptake, leading to additional warming after emissions were zeroed. Here, the time until atmosphere-ocean thermal equilibrium (i.e. the point at which temperatures stabilized) was observed at approximately 1000 years after zeroed emissions (Frolicher & Paynter, 2015). Over that time period, the warming commitment from past emissions was reported at 0.5 °C, leading to peak warming of approximately 2.5 °C above pre-industrial temperature (Frolicher & Paynter, 2015).

Though applying the ZEC concept to forcing from CO_2 yields the climate commitment resultant from the most dominant greenhouse gas, other greenhouse gas emissions and aerosols lead to a positive or negative additional radiative forcing on the climate system (Myhre et al., 2013). To address the climate commitment from historic forcing of all pollutants, ZEC scenarios have been used to show that the magnitude and sign of temperature change (warming or reversibility) are dependent on the combination of pollutants for which emissions cease (Matthews &Zickfeld, 2012; Allen et al., 2018b). Taking present-day as 2010, Matthews & Zickfeld (2012) calculated a warming commitment of approximately 0.1°C at 190 years (2200) after cessation of CO_2, aggregated non-CO_2 GHGs, and aerosol emissions. On a shorter, decadal timescale, this same simulation yielded a temperature increase of 0.3 °C, which was the peak temperature following zeroed emissions (Matthews & Zickfeld, 2012). This brief decadal warming period leading to peak temperature was caused by the immediate decline of aerosol concentrations (Matthews & Zickfeld, 2012). The subsequent warming reversibility of approximately 0.2 °C, leading to the long-term 0.1 °C warming commitment, was driven by diminishing concentrations of non-CO_2 GHGs (namely methane).

On an end-of-century (2100) timescale and by driving historic climate forcing from the same set of pollutants but setting those emissions to zero in 2018, Smith et al. (2019)[2] found a long-term warming reversibility of 0.2 °C. Similar to Matthews & Zickfeld (2012), they assessed the peak warming following zeroing all emissions at approximately 0.1 °C, thus yielding a long-term cooling relative to peak temperature of approximately 0.3 °C (Smith et al., 2019). The difference in these results is partially due to the differences in how the ERFs of CH_4 and N_2O were calculated as well as to internal differences in model structures (UVic-ESCM2.9 vs FAIR1.3) and length of ZEC. These studies are important because they describe the systems response, not only as a function of CO_2, but also by accounting for non-CO_2 GHGs and negative forcers such as aerosols.

Studies which model historical forcing rely on concentrations and emissions datasets from the historical, homogenized representative concentration pathways (RCPs) (van Vuuren et al., 2011; Meinshausen et al., 2011). A different historical modelling method to calculate the climate commitment is to use forcing output from a reanalysis dataset. From the HadCRUT4 reanalysis run to 2016, Mauritsen & Pincus (2017) developed a simple calculation based on the parameters that represent the Earth's climate system energy imbalance to estimate the climate commitment. Their results are therefore not reported after a length of time following zero emissions, but rather as measure of climate system equilibrium (Mauritsen & Pincus, 2017). When considering ocean carbon uptake after zero emissions of CO_2, aerosols and SLCFs, they estimated an equilibrium warming commitment of 0.26 ºC (Mauritsen & Pincus, 2017). Compared to the equilibrium

[2]This refers to results shown in Smith et al. (2019), Supplementary Figure 6, which is the same as from Allen et al., 2018b, Figure 1.5. The major difference between these studies is that Smith et al. (2019) directly compare their results to Matthews & Zickfeld (2012).

warming commitment of CO_2 alone, their estimated warming decreased after removing SLCFs and accounting for ocean carbon uptake (Mauritsen & Pincus, 2017).

2.4 The importance of non-CO_2 GHGs

Due to the variant lifetimes of non-CO_2 GHGs and the capacity of historical non-CO_2 GHG emissions to augment temperature change (Smith et al., 2012; Bowerman et al., 2013; MacDougall & Knutti, 2016), there is a need to better understand how non-CO_2 gases affect the ZEC on centennial timescales. Aside from their own source and sink cycles (see Chapter 2.2) one complication to warming driven by non-CO_2 GHGs increases atmospheric and ocean temperatures without participating directly in the carbon cycle (MacDougall & Knutti, 2016). This is problematic because their sinks are less sensitive than CO_2 to weakening from climate change. Reduced sensitivity to climate change is the result of the atmospheric sink of most non-CO_2 GHGs. That sink is a process of chemical reactions involving the hydroxyl radical (OH^-), whose abundance in the atmosphere is not directly influenced by temperature change (Levy, 1979; Seinfeld & Pandis, 2016). Some consequences for the carbon cycle by additional radiative forcing from non-CO_2 GHGs are: 1) increasing atmospheric temperature can inhibit plant growth without enhancing CO_2 fertilization (MacDougall & Knutti, 2016); 2) increasing temperature can increase soil organic carbon decomposition (MacDougall & Knutti, 2016); 3) this additional warming leads to lower rates of ocean CO_2 dissolution (MacDougall & Knutti, 2016); and 4) increased warming can reduce the capacity of the ocean to uptake heat from the atmosphere (Frolicher & Paynter, 2015).

Comparing how non-CO_2 GHGs and CO_2 emission affect temperature change, there is a difference in how temperature peaks before and after zero emissions. From CO_2 emissions alone,

peak temperatures are shown to occur within a decade after emissions cease and the delay is largely a result of the slow response of atmospheric temperature to ocean thermal inertia (Baede et. al, 2001; Hansen et al., 2005; Ricke & Caldiera, 2014; Zickfeld & Herrington, 2015). The timing of peak temperature following a single emission of CO_2 has been estimated at 10.1 years (Ricke & Caldiera, 2014), or decades longer for larger emissions (Zickfeld & Herrington, 2015). The relatively short lifetime of certain non-CO_2 GHGs, however, means their emissions cause warming prior to being zeroed (or prior to deep mitigation), but can lead to a decrease in temperature almost immediately afterwards (Bowerman et al., 2013). One of the consequences of this difference is that the rate of non-CO_2 emissions prior to peak CO_2 concentration can cause a temperature change threshold overshoot, where temperature changes exceed a target (e.g. 1.5 ^{o}C) and decline afterwards (Smith et al., 2012; Bowerman et al., 2013). That potential is highly relevant for policies seeking to stabilize temperature changes below a target and for mitigation scenarios involving net-negative emissions.

Looking specifically at how source sectors, including emissions from non-CO_2 GHGs, influence temperature change leading to the 1.5 ^{o}C threshold, the work from Mengis & Matthews (2019), assessed the individual net warming from fossil fuel combustion and land-use change /agriculture by partitioning emissions per source. Their results yielded a method where non-CO_2 GHG emissions can be partitioned to account for a specific sectors total emissions. Combining this idea with the principles of ZEC scenarios can yield estimates of the climate commitment associated with all CO_2 and non-CO_2 GHG emissions produced by fossil fuels and/or land-use change, giving results that are more accurately attributable to human activities. By assuming that groups of activities (for example LUC, including agriculture, and other anthropogenic activities) continues in the future and by zeroing emissions at present-day in the other sector (i.e. fossil fuel

combustion), the potential for past emissions from the eliminated sector and projected emissions from the continued sectors to increase temperature can be determined. Such analysis would render a baseline of the feasibility to continue activities in certain sectors while phasing out activities in the other.

CHAPTER 3

RESEARCH QUESTIONS

3.1 Research questions

My goal is to assess the contribution of non-CO_2 GHGs to the climate changes after emissions are set to zero, focussing both potential committed climate warming, as well as the reversibility of peak temperature changes caused by non-CO_2 emissions. I will expand on previous studies on this topic who have looked only at the aggregate effect of all non-CO2 gases together (Matthews & Zickfeld, 2012; Allen et al., 2018b); given that non-CO_2 GHGs have a large range of both forcing strength and persistence in the atmosphere, I will disaggregate non-CO_2 GHG warming to determine the climate commitment attributable to individual species as well as selected groupings of non-CO_2 GHGs. I will also expand on previous work that analyzed carbon cycle feedbacks from a methane-like gas, to further disaggregate those feedbacks by the non-CO_2 groupings (MacDougall & Knutti, 2016). In an attempt to capture climate system and carbon cycle feedbacks, I will use ZEC scenarios to simulate how climate changes over multiple centuries after the point of zero emissions.

Following the work of Mengis & Matthews (2019), I will further investigate the future climate changes that result from the all CO_2 and non-CO_2 emissions grouped by source category: (1) Fossil Fuel Combustion (FFC) and (2) land-use change (LUC, including agricultural activities). This analysis will yield a by-source analysis of the contribution of projected emissions from each of these two sector groupings (in the context of zeroed emissions in the other) to temperature change over long-term timescales

CHAPTER 4
METHODS

4.1 UVic-ESCM

All simulations were run using an updated version of the UVic-ESCM 2.9. Model tuning and forcing updates to align with CMIP6 protocols were performed by Nadine Mengis and Nesha Wright. To disaggregate non-CO_2 GHG forcing, a simple atmospheric chemistry module was implemented and constructed in the UVic-ESCM. This module follows the chemistry formulas used in FAIR 1.3, described by Smith et al. (2018) and includes new updates of methane and nitrous oxide forcing presented by Etminan et al. (2016). Additionally, the forcing parameters for CO_2 concentrations were updated to reflect these recent forcing changes.

For my atmospheric chemistry module, emissions from gases listed in Table 3.1 were used as input to calculate the atmospheric concentration of non-CO_2 GHGs over time. Each non-CO_2 GHG emissions time series was supplied in units mass per year (Meinshausen et al., 2011), which does not align with the UVic-ESCM emissions input units of mass per second. To align emissions time series to UVic-ESCM parameters, emissions were first converted into grams per second and then included as input data.

4.2 Atmospheric chemistry Module

In this atmospheric chemistry module, described in the following paragraphs and equations adapted from Smith et al. (2018)to fit UVic-ESCM parameters, a simple one-box atmosphere design was employed, with the sink of each non-CO_2 GHG calculated by an exponential decay of concentration anomaly as a function of gas lifetime. The radiative forcing for each gas was determined by its effective radiative forcing (ERF), which was calculated by the change in

concentration relative to pre-industrial scaled by the gases radiative efficiency. All emissions of non-CO_2 GHGs are assumed to be immediately well-mixed in the atmosphere.

This happens using the molar mixing ratio of each gas to convert emissions to atmospheric concentration (δC) via,

$$\delta C_t = \frac{E_t}{A_a} \frac{1}{(\omega_f/\omega_a)\rho_a d_z} \delta_t \quad \text{(Eq. 4.1)}$$

where E_t is the emissions of each gas (in units g s^{-1}), A_a is the atmospheric surface area (cm^2), ω_f is the molecular mass of the greenhouse gas, ω_a is the molecular mass of the dry atmosphere (28.97 g/mol) from Seinfeld & Pandis (2016), ρ_a is the density of the atmosphere at sea-level, d_z is the scale height of carbon (or height of the one-box atmosphere), and δ_t is the timestep (five days, in seconds).

The module updates the atmospheric concentration of each gas as a function of the input of new emissions, the concentration at the last time step and concentration decay by,

$$C_t = C_{t-1} + \frac{1}{2}(\delta C_{t-1} + \delta C_t) - C_{t-1}(1 - \exp(-1/\tau)) \quad \text{(Eq. 4.2)}$$

where, τ is the lifetime of each gas (Table 3.2), $\frac{1}{2}(\delta C_{t-1} + \delta C_t)$ is the average of emissions input between the last timestep and the current timestep, and $C_{t-1}(1 - \exp(-1/\tau)$ is the decay fucntion.

A difference between my module and that of Smith et al. (2018) is the treatment of CH_4 and N_2O natural emissions prior to 2005 (the RCP homogenization year). Smith et al. (2018) calculate time-varying natural emissions over the historical period to match observations from Meinshausen et al. (2011). After 2005, natural emissions are held constant at 202 Mt CH_4 yr^{-1} for CH_4 and 8.99 Mt $N_{2\text{-eq}}$ yr^{-1} for N_2O. For simplicity and because historical natural emissions of methane and nitrous oxide are uncertain, I followed the method of Meinshausen et al. (2011) and prescribed atmospheric concentrations for CH_4 and N_2O, as well as all other non-CO_2 GHGs, over

Table 4.1: *Reproduced from Smith et al. (2018).* GHG emissions modelled in this study. NI = not included. Index and unit (original) are based on the RCP datasets in Meinshausen et al. (2011). Unit (UVic-ESCM) is the conversion into UVic-ESCM units.

Index	Species	Unit (original)	Unit (UVic-ESCM)	Remark
0	Year	Year	Year	
1	CO_2 fossil	Gt C yr^{-1}	g C s^{-1}	
2	CO_2 land use	Gt C yr^{-1}	g C s^{-1}	
3	CH_4	Mt yr^{-1}	g s^{-1}	
4	N_2O	Mt N_2 yr^{-1}	g N_2 s^{-1}	
5	SO_x	Mt S yr^{-1}	g S s^{-1}	NI
6	CO	Mt yr^{-1}	g s^{-1}	
7	NMVOC	Mt yr^{-1}	g s^{-1}	
8	NO_x	Mt N yr^{-1}	g N s^{-1}	
9	BC	Mt yr^{-1}	g s^{-1}	NI
10	OC	Mt yr^{-1}	g s^{-1}	NI
11	NH_3	Mt yr^{-1}	g s^{-1}	NI
Florinated gases (F-gases) or Kyoto Protocol substances				
12	CF_4	kt yr^{-1}	g s^{-1}	
13	C_2F_6	kt yr^{-1}	g s^{-1}	
14	C_6F_{14}	kt yr^{-1}	g s^{-1}	
15	HFC23	kt yr^{-1}	g s^{-1}	
16	HFC32	kt yr^{-1}	g s^{-1}	
17	HFC43-10	kt yr^{-1}	g s^{-1}	
18	HFC125	kt yr^{-1}	g s^{-1}	
19	HFC134a	kt yr^{-1}	g s^{-1}	
20	HFC143a	kt yr^{-1}	g s^{-1}	
21	HFC227ea	kt yr^{-1}	g s^{-1}	
22	HFC245fa	kt yr^{-1}	g s^{-1}	
23	SF_6	kt yr^{-1}	g s^{-1}	
Ozone depleting substances (ODS) or Montreal Protocol gases				
24	CFC-11	kt yr^{-1}	g s^{-1}	
25	CFC-12	kt yr^{-1}	g s^{-1}	
26	CFC-113	kt yr^{-1}	g s^{-1}	
27	CFC-114	kt yr^{-1}	g s^{-1}	
28	CFC-115	kt yr^{-1}	g s^{-1}	
29	CCl_4 (carb-tet)	kt yr^{-1}	g s^{-1}	
30	Methyl chloroform (mcf)	kt yr^{-1}	g s^{-1}	
31	HCFC22	kt yr^{-1}	g s^{-1}	
32	HCFC141b	kt yr^{-1}	g s^{-1}	
33	HCFC142b	kt yr^{-1}	g s^{-1}	
34	Halon 1211	kt yr^{-1}	g s^{-1}	
35	Halon 1202	kt yr^{-1}	g s^{-1}	
36	Halon 1301	kt yr^{-1}	g s^{-1}	
37	Halon 2402	kt yr^{-1}	g s^{-1}	
38	CH_3Br	kt yr^{-1}	g s^{-1}	
39	CH_3Cl	kt yr^{-1}	g s^{-1}	

the historical period. Beyond 2005, I adopted the constant natural emissions of CH_4 and N_2O from Smith et al. (2018) and included those as an addition to atmospheric concentration at each time step, thus rendering,

$$C_t = C_{t-1} + \frac{1}{2}(\delta C_{t-1} + \delta C_t) - C_{t-1}(1 - \exp(-1/\tau)) + \delta C_{nat} \quad \text{(Eq. 4.2b)}$$

where C_{nat} is the natural emissions converted to atmospheric concentration via Eq. 1.

As described above (Chapter 2.4), the sink of many non-CO_2 GHGs is an oxidation process involving the hydroxyl radicle (OH^-). From fossil fuel sources, the oxidation of CH_4 produces small quantities of CO_2. This process constitutes a positive feedback of CH_4 concentration to CO_2 concentration by,

$$E_{CH_4 \to CO_2} = 0.61 f_{CH_4 fos}(C_{CH_4} - C_{CH_4,pi})(1 - \exp(-1/\tau_{CH_4}) \quad \text{(Eq. 4.3)}$$

where $f_{CH_4 fos}$is the fraction of methane emissions from fossil fuel sources, taken as 32.1% as per the Global Methane Budget (Saunois et al., 2016), and 0.61 is the percentage of methane concentration anomaly oxidized into carbon dioxide. In my module, this feedback is applied when the option to include CH_4 emissions is turned on and is always greater than or equal to zero.

Another product of CH_4 decay is stratospheric water vapor. Here this decay leads to an additional radiative forcing that is modelled as 12% of the methane ERF in a given time step.

A recent update by Etminan et al. (2016) showed that CO_2, CH_4, and N_2O share radiative forcing band overlaps. These updates were included in my module and are reproduced here. In Eqs 4-6, *C* represents CO_2 concentration (ppmv), and *M* and *N* represent CH_4 and N_2O concentration (ppbv).

$$F_{CO_2} = [(-2.4 \times 10^{-7})(C - C_{pi})^2 + (7.2 \times 10^{-4})|C - C_{pi}| - (1.05 \times 10^{-4})(N + N_{pi}) + 5.36] \times \log\left(\frac{C}{C_{pi}}\right) \quad \text{(Eq. 4.4)}$$

$$F_{N_2O} = [(-4.0 \times 10^{-6})(C + C_{pi}) + (2.1 \times 10^{-6})(N + N_{pi}) - (2.45 \times 10^{-6})(M + M_{pi}) + 0.117] \times (\sqrt{N} - \sqrt{N_{pi}}) \quad \text{(Eq. 4.5)}$$

$$F_{CH_4} = \left[-(6.5 \times 10^{-7})(M + M_{pi}) - (4.1 \times 10^{-6})(N + N_{pi}) + 0.043\right] \times \left(\sqrt{M} - \sqrt{M_{pi}}\right)$$
(Eq. 4.6)

Table 4.2: *Reproduced from Smith et al. (2018).* All lifetimes and radiative efficiencies, except methane, are from AR5 (Myhre et al., 2013, Table 8.A.1). For gases with a listed radiative efficiency, the effective radiative forcing is calculated using a linear function of concentration.

Gas	Molecular weight ω_f (g mol^{-1})	Radiative efficiency η(W m^{-2} ppb^{-1})	Lifetime τ(yr)	r_i	n_{Cl}	n_{Br}
Major gases						
CH_4	16.04	N/A	9.6			
N_2O	44.01	N/A	121			
F-gases						
CF_4	88.00	0.09	50 000			
C_2F_6	138.01	0.25	10 000			
C_6F_{14}	338.04	0.44	3100			
HFC23	70.01	0.18	222			
HFC32	52.02	0.11	5.2			
HFC43-10	252.06	0.42	16.1			
HFC125	120.02	0.23	28.2			
HFC134a	102.03	0.16	13.4			
HFC143a	84.04	0.16	47.1			
HFC227ea	170.03	0.26	38.9			
HFC245fa	134.05	0.24	7.7			
SF_6	146.06	0.57	3200			
ODS						
CFC-11	137.37	0.26	45	0.47	3	0
CFC-12	120.91	0.32	100	0.23	2	0
CFC-113	187.38	0.30	85	0.29	3	0
CFC-114	170.92	0.31	190	0.12	2	0
CFC-115	154.47	0.20	1020	0.04	1	0
carb-tet	153.81	0.17	26	0.56	4	0
mcf	133.40	0.07	5	0.67	3	0
HCFC22	86.47	0.21	11.9	0.13	1	0
HCFC141b	116.94	0.16	9.2	0.34	2	0
HCFC142b	100.49	0.19	17.2	0.17	1	0
Halon 1211	165.36	0.29	16.0	0.62	1	1
Halon 1202	209.82	0.27	2.9	0.62	0	2
Halon 1301	148.91	0.30	65	0.28	0	1
Halon 2402	259.82	0.30	20	0.65	0	2
CH_3Br	94.94	0.004	0.8	0.60	0	1
CH_3Cl	50.49	0.01	1	0.44	1	0

For all other non-CO_2 GHGs a linear equation was used to describe their effective radiative forcing. This equation is dependent on the change in concentration since pre-industrial for each gas, where η_i is the radiative efficiency for each gas listed in Table 4.2.

$$F_i = \eta_i\left(C_i - C_{i,pi}\right); i \in \qquad \text{(Eq. 4.7)}$$

The modelling of radiative forcing from tropospheric ozone was here calculated via ozone forming pre-cursor concentration of CH_4, and emissions of carbon monoxide (CO), non-methane volatile organic compounds (NMVOC), and nitrogen oxides (NO_x). A linearity was assumed between atmospheric concentration of methane and ozone forcing.

$$F_{O_3tr} = \beta_{CH_4}\left(C_{CH_4} - C_{CH_4,pi}\right) + \beta_{NO_x}\left(E_{NO_x} - E_{NO_x,pi}\right) + \beta_{CO}\left(E_{CO} - E_{CO,pi}\right) + \beta_{NMVOC}\left(E_{NMVOC} - E_{NMVOC,pi}\right) \quad \text{(Eq. 4.8)}$$

The coefficients β are provided in Table 4.3. Smith et al. (2018) employ a switch for coefficient values in 1850. Since my simulations all began in year 1850, only the post-1850 coefficients were employed in my module.

The ERF for stratospheric ozone was calculated using the exponential relationship:

$$F_{O_3st} = a(b\,s)^c \quad \text{(Eq. 4.9)}$$

where $a = -1.46\text{x}10^{-5}$, $b = 2.05\text{x}10^{-3}$, and $c = 1.03$. s represents the equivalent effective stratospheric chlorine, and is a measure of the contribution of each ozone depleting substance to chlorine and bromine atoms in the stratosphere, calculated by

$$s = r_{CFC-11} \sum_{i \in ODS} \left(n_{Cl}(i) C_i \frac{r_i}{r_{CFC-11}} + 45 n_{Br}(i) C_i \frac{r_i}{r_{CFC-11}} \right) \quad \text{(Eq. 4.10)}$$

where r_i is the fractional release of each compound, and n_{Cl} and n_{Br} are the number of chlorine and bromine atoms in each gas. The factor 45 is included to represent that bromine is 45 times more effective at reducing stratospheric ozone than chlorine.

Table 4.3: Parameters for contribution to tropospheric ozone ERF from each precursor (*adapted from Smith et al. (2018)*. Coefficient and pre-industrial values are here reported as is in Smith et al. (2018) but were converted to UVic-ESCM units.

Ozone forcing efficiency (Eq. 8)		
Species	Post-1850 (β_i)	Pre-industrial value
CH_4	1.73 x 10^{-4} W m^{-2} ppb^{-1}	722 ppb
CO	8.51 x 10^{-5} W m^{-2} (Mt yr^{-1})$^{-1}$	170 Mt CO yr^{-1}
NMVOC	2.25 x 10^{-4} W m^{-2} (Mt yr^{-1})$^{-1}$	5 Mt NMVOC yr^{-1}
NO_x	9.08 x 10^{-4} W m^{-2} (Mt yr^{-1})$^{-1}$	2 Mt N yr^{-1}

4.3 Atmospheric chemistry module validation

Because the atmospheric chemistry module does not include feedbacks from other components of the UVic-ESCM a full model validation is not necessary. With respect to the atmospheric chemistry module, over the historic period (1850-2005) in all simulations the model was driven by prescribed concentrations of greenhouse gases. Theses concentrations were input from yearly data as per the RCP historical GHG concentrations dataset (Meinshausen et al., 2011). In the UVic-ESCM this yearly input data was interpolated to five-day time steps internally in the model. For each time step the concentration anomaly from pre-industrial value was used to calculate radiative forcing of each non-CO_2 GHG**.** Except for the time step difference, this procedure is the same as that used to simulate and validate historical forcing in FaIR 1.3 (Smith et al., 2018). Over the historical period, the non-CO_2 GHGs showed radiative forcing in line with that of FaIR 1.3 and as such the radiative forcing equations should be viewed as valid.

In the near-present (2005-2019) most simulations (expect the by-source simulations) were driven by input of non-CO_2 GHG emissions under RCP4.5. The atmospheric chemistry module then calculated the concentration in each time step, which was used to calculate the effective radiative forcing for each gas per time step. Owing to the difference in time steps between the UVic-ESCM and FaIR 1.3 a slight difference in the calculated yearly concentration of non-CO_2 GHGs was observed between these two models. This difference, however, is fractional which means the values of atmospheric concentration are almost the same, or as expected.

4.4 Land-use change and agriculture

In the by-source simulations (see Chapter 5.2.2), I model how the climate system would evolve in the absence of land-use change and agriculture emissions. Due to how the UVic-ESCM

models the spatial components of agriculture, there are some limitations to this simulation. In the UVic-ESCM agriculture activities are modelled from an input of a spatial dataset where each grid cell in the dataset represents the fraction of that land area which is used for agriculture. Under natural circumstances, if land-use change and agriculture activities were to stop, crop land would return to forest. Greater tree cover would draw more carbon out of the atmosphere and increase the land carbon pool. In my simulations, I assume there is no change in the spatial portion of land-use change and agriculture since their pre-industrial levels. Only the emissions of land-use change and agriculture activities, taken as a portion of emissions under RCP4.5 are modelled in my simulations.

CHAPTER 5

MANUSCRIPT

5.1 Introduction

An objective of the Paris Agreement is to attempt to prevent global temperature from exceeding 1.5 °C above pre-industrial levels (UNFCCC, 2015). Current understanding of the climate system and carbon cycle suggests such global warming is driven primarily by cumulative carbon dioxide (CO_2) emissions (Solomon et al., 2009; Gillett et al., 2013; Matthews & Solomon, 2013; Allen & Stocker, 2014; Millar et al., 2016; Matthews et al, 2017; Millar et al., 2017). However, non-CO_2 greenhouse gases and aerosols are also significant drivers of global temperature changes (Smith et al., 2012; Bowerman et al., 2013). CO_2-induced warming has been shown to persist on timescales of a century to multiple-millennia, meaning the global temperature change caused by past and current CO_2 emissions does not decline during the foreseeable future (Matthews & Zickfeld, 2012; Allen et al., 2018b). In contrast, warming caused by non-CO_2 greenhouse gases with shorter atmospheric lifetimes, does not persist as long as that caused by CO_2 and can therefore be reversed with ambitious mitigation efforts (Matthews & Zickfeld, 2012; Bowerman et al., 2013).

In effect, the future climate system is committed to warming, and other impacts, from past emissions, which is referred to as the warming commitment from past emissions (Matthews & Zickfeld, 2012). This warming commitment can be estimated by modelling how the climate system reacts to a given amount of human induced climate forcing from greenhouse gases (GHGs) and aerosols, then setting emissions from those pollutants to zero and continuing the model for centuries or multiple-millennia in the absence of additional emissions (Matthews et al., 2012; Zickfeld et al., 2017; Allen et al., 2018b). This approach yields an estimate of the "Zero Emissions

Commitment" (ZEC), which defines the change in future temperature that results after zero emissions. In the case of CO_2-only emissions, when emissions are zeroed, the physical processes of ocean heat uptake and the efficacy of sinks for atmospheric CO_2 strike a balance to yield a nearly constant global temperature (Solomon et al., 2009; Matthews & Zickfeld et al., 2012; Frolicher et al., 2014; Ehlert & Zickfeld, 2015).

Estimates of the CO_2-only ZEC typically vary between ±0.5 °C (Solomon et al., 2009; Matthews & Zickfeld, Allen et al., 2018b). Two drivers behind these differing values are: the cumulative carbon emissions at the time of ZEC; and the combination of human induced emissions that are zeroed or not. For example, in a study assessing high atmospheric CO_2 burden, Ehlert & Zickfeld (2017) found a maximum warming commitment from a CO_2-only ZEC scenario of 0.9 °C with the remaining simulations yielding a climate commitment between 0 and 0.5 °C. Analyses of the influence of aerosols on warming commitment, where aerosol emissions are zeroed along with CO_2, have shown a long-term warming commitment of 1.2 or 0.5 °C (Matthews & Zickfeld, 2012; Allen et al., 2018b, respectively). In experiments where non-CO_2 GHGs are zeroed along with CO_2 and aerosols emissions are held constant, a negative ZEC has been reported (Matthews & Zickfeld, 2012; Allen et al., 2018b).

A limitation of the studies that zero non-CO_2 GHGs is that the contribution to global temperature change from each gas is aggregated into one parameter (Matthews & Zickfeld, 2012; Allen et al., 2018b). These gases exhibit unique atmospheric lifetimes, concentrations, and radiative efficiencies, which are the factors of a gases effective radiative forcing (ERF) (Smith et al., 2012; Allen et al., 2018a; Smith et al., 2018). Aggregating non-CO_2 GHGs into a single climate forcing parameter masks the ERF of certain gases and thus their influence on the climate system. Some non-CO_2 GHGs, for example, have low atmospheric concentrations but long lifetimes,

meaning an emission marginally affects global temperature over multiple-millennia (Smith et al., 2012). Others exhibit shorter lifetimes but higher radiative efficiency and concentration, meaning an emission causes significant immediate temperature change but might not cause lasting change to climate system (Bowerman et al., 2013; MacDougall et al., 2015).

Coinciding with the differentiating influence of specific non-CO_2 GHGs on global warming is the fact that GHGs are often co-emitted by the same source (Rogelj et al., 2014; Mengis & Matthews, 2019). At a broad level, the two main sources of emissions are from fossil fuel combustion (FFC) and land-use change including agriculture (LUC) (Baede et al., 2001; Myhre et al., 2013; Saunois et al., 2016; Le Quere et al., 2018). Recent work has shown that by partitioning emissions by source, the net influence of these human activities on global warming can be captured (Mengis & Matthews, 2019). That influence was shown by Mengis & Matthews (2019) to have a substantial impact on the size of the remaining carbon budget for the 1.5 °C temperature target.

As policy measures to keep global temperature below 1.5 °C will require multi-faceted reductions in emissions, there is a need to better assess the ZEC and reversibility of peak temperature change from non-CO_2 GHGs. My study fills this gap by investigating the ZEC from individual and policy-relevant groupings of non-CO_2 GHGs. I further partition GHGs by sector to examine the future warming associated with all emissions from fossil fuel combustion and land-use change and agriculture. In these analyses I use different terms to differential between the sign (positive or negative) of temperature change following zero emissions. Here I use the term warming commitment refer to a positive temperature change after zero emissions, warming reversibility to refer to a negative temperature change after zero emissions, and climate commitment to refer more generally to either of these two cases.

5.2 Model and Simulations

5.2.1 Model

All simulations were carried out using an updated version of the University of Victoria Earth System Model version 2.9 (UVic-ESMC 2.9), an Earth-system model of intermediate complexity (EMIC). The UVic-ESCM 2.9 includes an atmospheric energy-moisture balance model, general ocean circulation model, land surface model, and dynamic sea-ice model (Weaver et al., 2001; Eby et al., 2009; Wania et al., 2013). It simulates an integrated global carbon cycle with carbon fluxes coupled between land, ocean, and ocean sediment. The energy-moisture balance model is a vertically integrated representation of the atmosphere, housing feedbacks from water vapour, planetary long wave radiation, and dynamic wind. A resolution of 1.8° (longitudinal) x 3.6° (latitudinal) is used in all components.

The version of the UVic-ESCM 2.9 used here has been updated to include a description of the permafrost carbon pool (MacDougall & Knutti, 2016), with updated forcing following CMIP6 protocols (Mengis, 2019). For the simulations carried out here, a simple non-CO_2 GHG atmospheric chemistry module was added to the UVic-ESCM. This module represents the effective radiative forcing (ERF) from non-CO_2 GHGs either using prescribed concentrations, or with prescribed emissions which are then used to calculate concentrations and radiative forcing. For each gas an ERF parameter is applied as a function of changes in atmospheric concentration relative to pre-industrial levels and radiative efficiency to yield the radiative forcing for that species (Etminan et al., 2016; Smith et al., 2018). These equations cover forcing from methane (CH_4), nitrous oxide (N_2O), fluorinated gases (F-gases, or Kyoto Protocol gases), ozone depleting substance (ODS, or Montreal gases), stratospheric ozone, stratospheric water vapour via CH_4 decay, and tropospheric ozone via carbon monoxide (CO), non-methane volatile organic carbon

(NMVOC), nitrogen oxides (NOx) emissions, and change in CH_4 concentration (Smith et al, 2018). In these equations, the sink of non-CO_2 GHGs is described by their atmospheric lifetime, where a fraction of (CH_4) emissions decay into CO_2, thus increasing atmospheric CO_2 concentration.

Effective radiative forcing (ERF) for each gas is calculated as a function of the change in atmospheric concentration relative to pre-industrial and given values of radiative efficiency (Etiman et al., 2016; Smith et al., 2018). Since, in the simple model setup, the atmospheric decay of these species is by means of their lifetime; as a result, gases with shorter lifetimes exhibit faster decreases in concentration after zeroed emissions (Smith et al., 2018). The response of ERF per gas to zeroed emissions is thus directly related to the atmospheric lifetime of the gas in question.

One exception is CH_4 and N_2O, which are known exhibit a long-wave radiation absorption overlap. Nitrous oxide shares an additional absorption band overlap with CO_2 (Etminan et al., 2016). This absorption band overlap means the ERFs of methane and nitrous oxide are co-dependent on the concentration changes of either gas. If CH_4 concentration is higher, as is the case immediately following zero emissions, there should be a reduction in the ERF of N_2O over that period. Compared to the CH_4& N_2O simulation, the ERF of N_2O in the N_2O alone simulation shows an average 1.4% increase between 2020 and 2030. This average percent increase declines to negligible by the end of the century, when CH_4 has returned to pre-industrial and when the addition of CH_4 decay into CO_2 is no longer a factor of CO_2 concentration. Despite this small reduction in the individual ERF of N_2O, the CH_4& N_2O simulation shows higher combined effective radiative forcing than the simulation for either gas alone.

5.2.2 Simulations

My analysis uses ZEC scenarios to investigate the long-term climate commitment from past non-CO_2 emissions. Climate commitments on the century timescale looked at here can be used to relate past non-CO_2 emissions to the reversibility of peak temperature. On these timescales the impact of aerosol emissions on temperature change is less important. The effect of historic aerosol emissions is to reduce peak warming (Myhre et al., 2013), but long-term temperature change is driven by CO_2 and long-lived non-CO_2 GHGs (Matthews & Zickfeld, 2012; Allen et al., 2018b). In ZEC scenarios where historical aerosol emissions are included and zeroed along with CO_2 and other gases, models show an initial warming period during the first decade after zero emissions caused by the rapid decline in atmospheric aerosol concentration (Matthews & Zickfeld, 2012; Allen et al., 2018b). To limit the noise from that initial warming and to focus on long-term temperature change, the historical aerosol forcing was removed from my scenarios.

To disaggregate the ZECs of non-CO_2 GHGs, separate simulations were carried out for individual and groups of gases. Non-CO_2 GHGs were grouped as follows: CH_4-only, N_2O-only, CH_4 and N_2O together, F-gases, ODSs, and tropospheric ozone (trop-ozone). Each non-CO_2 GHG simulation also includes prescribed concentrations or emissions of CO_2 to yield a forcing relative to CO_2 and similar to that of present-day (Haustein et al., 2017). As a control, a simulation with anthropogenic forcing from prescribed CO_2 concentrations was also run. The climate commitment of each individual gas or grouping of gases is therefore represented as the difference between their respective simulation and the CO_2-only simulation.

Additionally, two further simulations were run, where emissions of CO_2 and co-emitted non-CO_2 emissions were prescribed according to source category: one for FFC emissions and the other for LUC emissions. In these, emissions from CH_4, N_2O and tropospheric ozone were partitioned using mean estimates of proportional contribution to total forcing per gas from Mengis

& Matthews (2019) (see Table 5.1), while CO_2 emissions were taken from historical and RCP4.5 partitions (Meinshaunsen et al., 2011).

Table 5.1: The partitioning of anthropogenic non-CO_2 GHGs. *Table is a partial re-production of Table 1 from Mengis& Matthews (2019).* Reported are only the means and excluding the uncertainty ranges.

Partitioning of anthropogenic non-CO_2 forcing in %			
	Source		
Emission	FFC	LUC (agriculture + biomass burning)	Other anthropogenic activities
CH_4	28	38 + 11	23
Stratospheric water vapor from CH_4	28	38 + 11	23
N_2O	10	60 + 10	20
Tropospheric-ozone	51	39	10

Simulations were run over the historical period (1850-2005) using prescribed GHG concentrations from the RCP historical concentration dataset (Meinshaunsen et al., 2011). GHG emissions from RCP4.5 were used to approximate anthropogenic radiative forcing to the present-day period (2005-2019), which closely follows current emissions trends (Haustein et al., 2017; Le Quéré et al. 2018). Starting in 2020 radiative forcing was projected by setting relevant GHG emissions to zero and allowing their concentrations to decline according to the results of the carbon cycle and atmospheric chemistry modules. For the FFC and LUC simulations, both source emissions and emissions from other anthropogenic activities were included during the historic-to-present-day period. In the FFC run, starting in 2020, LUC emissions were set zero and the FFC and other anthropogenic emissions were allowed to continue following RCP4.5 projections. Similarly, in the LUC run, FFC emissions were set to zero and the LUC and other anthropogenic emissions were allowed to continue. I did not include aerosol emissions in any simulations; as a result, these results quantify the warming commitment associated with CO_2 and non-CO_2 greenhouse gas emissions only.

5.2.3 Calculations

To assess the long-term climate commitment from historical non-CO_2 GHG emissions, the percent temperature change from peak temperature remaining was calculated. This is defined as the fraction of peak warming remaining for each individual gas or gas grouping relative to CO_2. It was calculated by,

$$\%\mathrm{T}(t) = \frac{(SAT_{i,t} - SAT_{CO_2,t})}{(SAT_{i,max} - SAT_{CO_2,max})} \times 100\% \qquad \text{(Eq. 5.1)}$$

where, $SAT_{i,t}$ is the temperature per simulation (i) in time (t), and $SAT_{i,max}$ is the peak temperature during simulation (i)

5.3 Results

5.3.1 Historical and zero emissions temperature commitment

Figure 5.1 shows the change in ERF after zero emissions for the two dominant non-CO_2 GHGs (CH_4 and N_2O) (Myhre et al., 2013), as well as specific gases from the other main GHG groups (F-gases and ODS's) and tropospheric-ozone. Additionally, these gases cover the range of atmospheric lifetimes of non-CO_2 GHGs (Smith et al., 2012; Smith et al., 2018), with the exception of tropospheric ozone, whose atmospheric lifetime is on the order of days (Myhre et al., 2013) and whose concentration is not calculated in this model (see Eq. 8). Atmospheric lifetimes for the gases shown in Figure 5.1 span decades to multiple millennia; with CH_4 at 9.3 years, N_2O at 121 years, CF_4 at 50,000 years, and CFC-11 at 45 years.

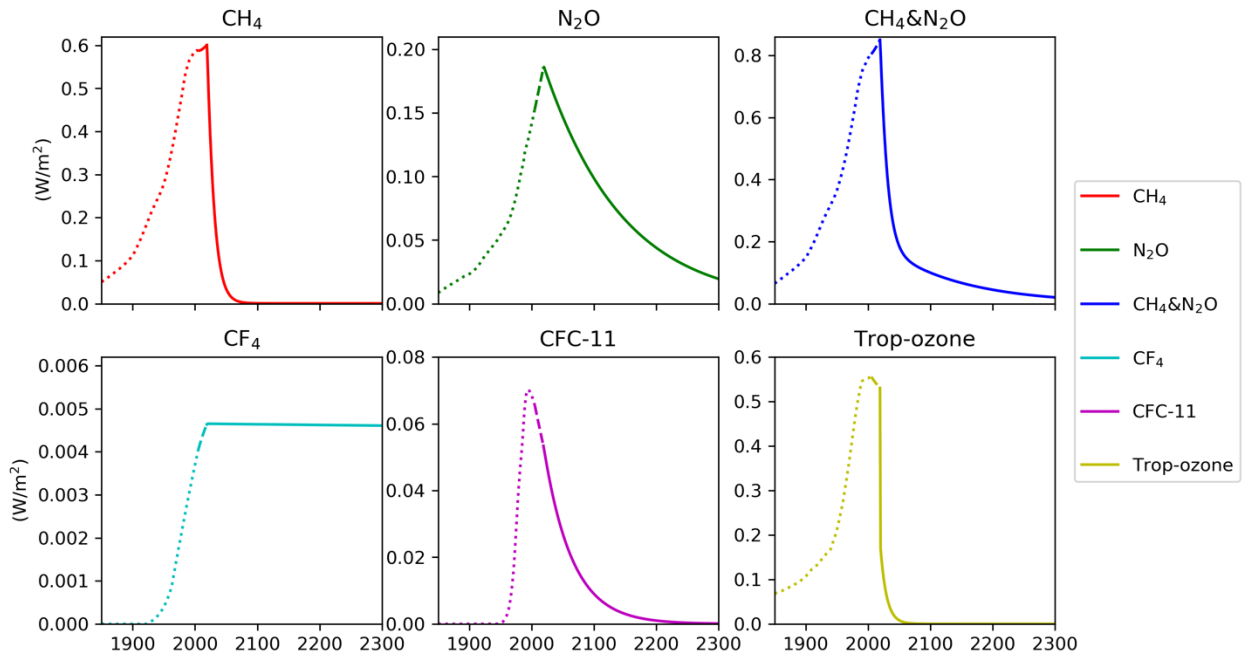

Figure 5.1: Historical and projected effective radiative forcing (W/m²) of CH_4, N_2O, CH_4& N_2O, CF_4, CFC-11, and tropospheric-ozone. Plots show the change in radiative forcing relative to 1850. Dotted lines (1850-2005) represent forcing from prescribed concentration; dashed lines (2005-2019) represent forcing from concentrations calculated as a function of emissions from the RCP4.5 scenario; and solid lines represent projected forcing from concentrations calculated as a function zero emissions

Though CH_4 produces the most ERF over the historical to present-day period (excluding the CH_4& N_2O ERF), its shorter atmospheric lifetime results in a return of atmospheric abundance to pre-industrial levels for the species within less than half a century after zeroed emissions thereby causing a steep decline in ERF following zeroed emissions.

In contrast, the multi-millennial atmospheric lifetime of CF_4 yields an ERF that remains approximately constant in the centuries after emissions cessation. The difference in rates of decline in ERF (solid lines) between N_2O and CFC-11 can be explained by both the difference in the pre-industrial concentrations of those gases and the difference in the rate of increase in concentration over the historical to present-day period (dotted line). N_2O has a pre-industrial concentration of approximately 272 parts per billion by volume (ppbv) and increases to 316 ppbv by 2000, whereas

CFC-11 has no pre-industrial concentration and increases to approximately 264 parts per trillion by volume (pptv) between 1950 and 2000 (Meinshausen et al., 2011).

The inclusion of CO_2 in all simulations both yields a temperature approximate to the present-day and functions as a control against which to calculate the effect of individual and groups of non-CO_2 gases. Figure 5.2 displays the change in SAT relative to 1850 for each non-CO_2 scenario and for CO_2 alone.

Over the historical to present-day period, the most dominant change in SAT is in scenarios

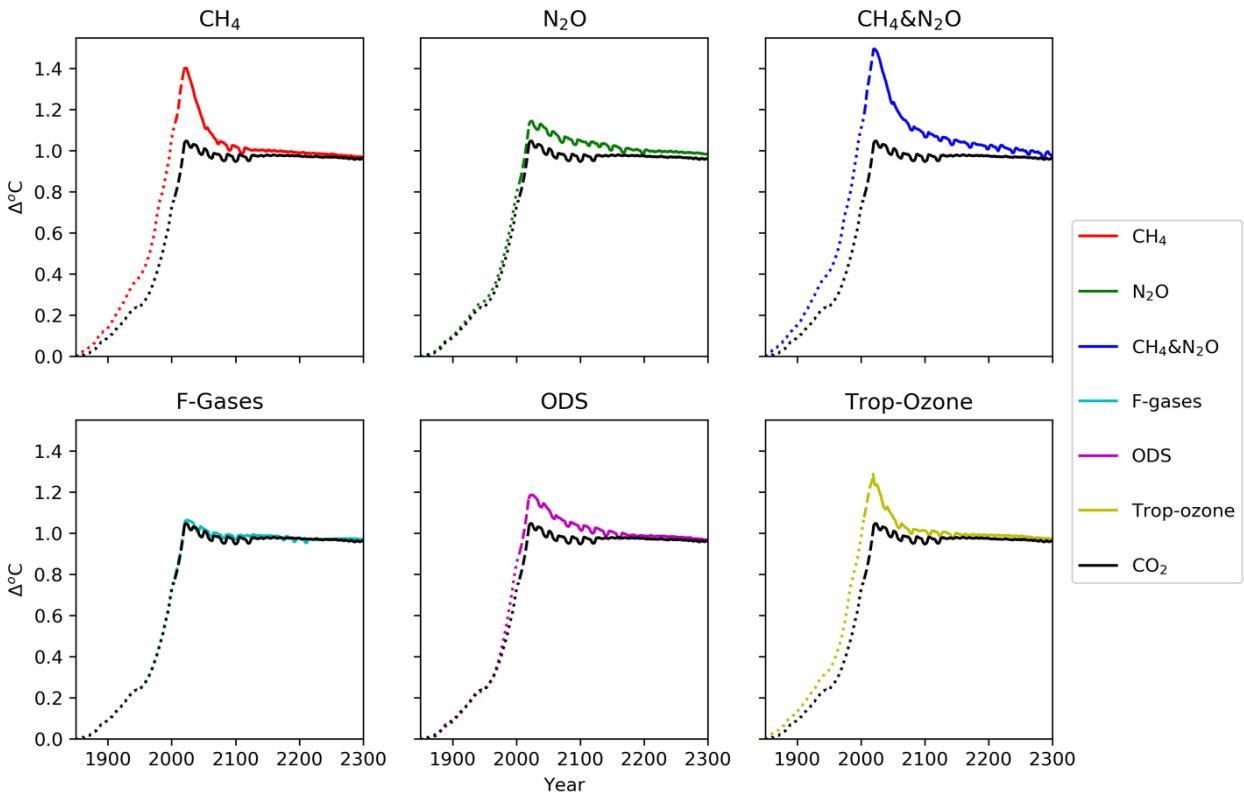

Figure 5.2: The change in SAT relative to 1850 for individual and groups of non-CO_2 GHGs. For a control reference the change in SAT in a simulation forced only by CO_2 is displayed on each plot. Dotted lines represent change in SAT as a function of prescribed concentrations, dashed lines represent change in SAT as a function of emissions from RCP4.5, and solid lines represent change in SAT as a function of zeroed emissions. Each non-CO_2 GHG scenario is also forced by CO_2.

forced by CH_4.The difference in the historical change in SAT between scenarios with CH_4 and those without is primarily a difference in the change in historical concentration of CH_4 compared to the other GHG species, which follows the same trend as seen in Figure 5.1. Due, again, to the short atmospheric lifetime of CH_4, in scenarios with CH_4 SAT declines rapidly following zero

emissions. In the remaining scenarios, the long-term trajectory of SAT change after zeroed emissions more closely follows that of CO_2.

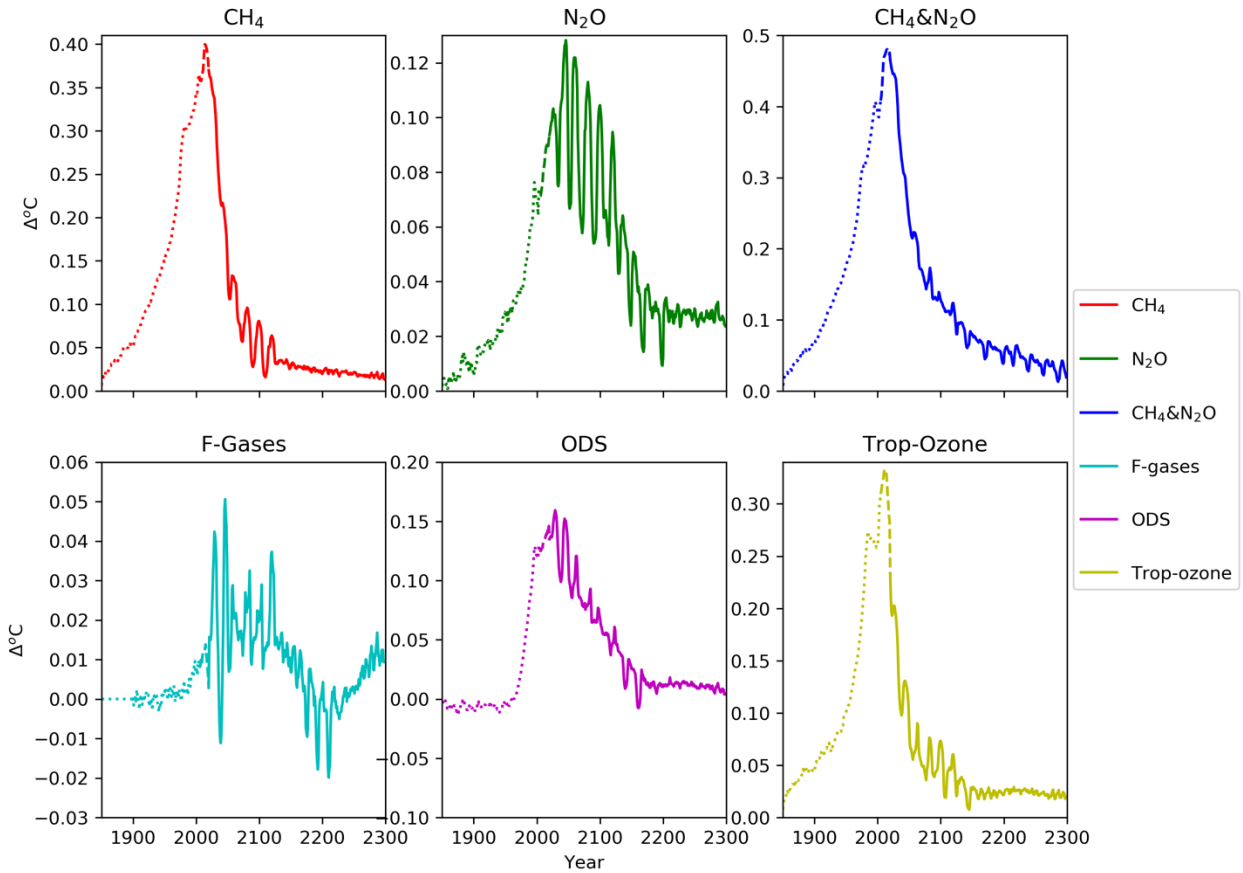

Figure 5.3: Historical and projected temperature change per gas or gas grouping relative to the historic and projected temperature change of a simulation forced by CO_2 only. Dotted lines show historic temperature change to 2005, dashed lines show temperature change from 2005 to 2019 (when emissions were zeroed), and solid lines show temperature change following zeroed emissions.

Figure 5.3 shows the historical and long-term temperature change following zero emissions for individual and groupings of non-CO_2 GHGs relative CO_2. Over the historical period, CH_4 alone is responsible for approximately 0.4 ºC warming, where N_2O alone accounts for 0.1 ºC warming. Owing to the absorption band overlap reducing the historical ERF of CH_4 and N_2O in the CH_4& N_2O simulation, the historical temperature change from CH_4 and N_2O combined is 0.48 ºC, marginally less than if SAT change was aggregated between the CH_4 and N_2O only simulations.

Tropospheric-ozone here yields 0.33 ºC historical warming, with ODSs yielding 0.16 ºC historic warming and F-gases yield negligible historic warming.

Table 5.2 displays the average historical warming per individual and gas groupings in each decade between 1950 to 2019. Gases with greater emissions over the historical period, CO_2, CH_4, trop-ozone are the most responsible for historical warming. Both, CH_4 and trop-ozone have short atmospheric lifetimes, and as a result the historical warming caused by those gases rapidly declines following zero emissions. Evident from Figure 5.3, the rate of temperature decline in CH_4 driven scenarios is higher than all scenarios other than trop-ozone. This rate of temperature decline is the highest for CH_4in the second decade after ZEC, where temperatures decline at approximately 0.01 ºC per year in that decade.

Table 5.2: Average SAT change per gas or gas groupings relative to 1850. Temperature change for Non-CO_2 gases is reported relative to CO_2

Average SAT change per decade ºC							
	Year ranges						
Gases	1950-1960	1960-1970	1970-1980	1980-1990	1990-2000	2000-2010	2010-2019
CO_2	0.26	0.31	0.39	0.50	0.64	0.78	0.92
CH_4	0.16	0.20	0.26	0.30	0.32	0.36	0.39
N_2O	0.03	0.03	0.04	0.05	0.07	0.07	0.09
CH_4 & N_2O	0.19	0.23	0.30	0.34	0.39	0.42	0.48
F-gases	0.0	0.0	0.0	0.0	0.0	0.0	0.01
ODSs	0.0	0.0	0.02	0.07	0.11	0.13	0.14
Trop-ozone	0.11	0.14	0.19	0.26	0.26	0.30	0.31

Over the long-term, 2020-2300, the temperature commitment for each gas and gas grouping declines to zero. This net cooling after zero emissions ranges between 0.45 and 0 ºC. The greatest cooling following zeroed emissions is from scenarios including CH_4, where again the brief atmospheric lifetime of CH_4 leads to a rapid reduction concentration after emissions cessation.

5.3.2 Peak temperature reversibility

With the exception of tropospheric-ozone, all simulations show an increase in warming up to or shortly after the point of zero emissions and all simulations show cooling afterwards. This indicates that the historical temperature increase of each non-CO_2 GHG and gas grouping reported in Table 5.2 can be reversed. The difference with the tropospheric ozone simulation is that following RCP4.5, precursor emissions from CO, NMVOCs and NOx begin to decline in 2012 and SAT is thus declining by the time of ZEC (Meinshausen et al., 2011). Additionally, because the tropospheric ozone ERF is calculated as a function of precursor emissions and not concentrations of those pollutants, the ERF begins a sharp decline in the first time step after ZEC, therefore causing the highest rate of cooling as shown in Figure 5.3.

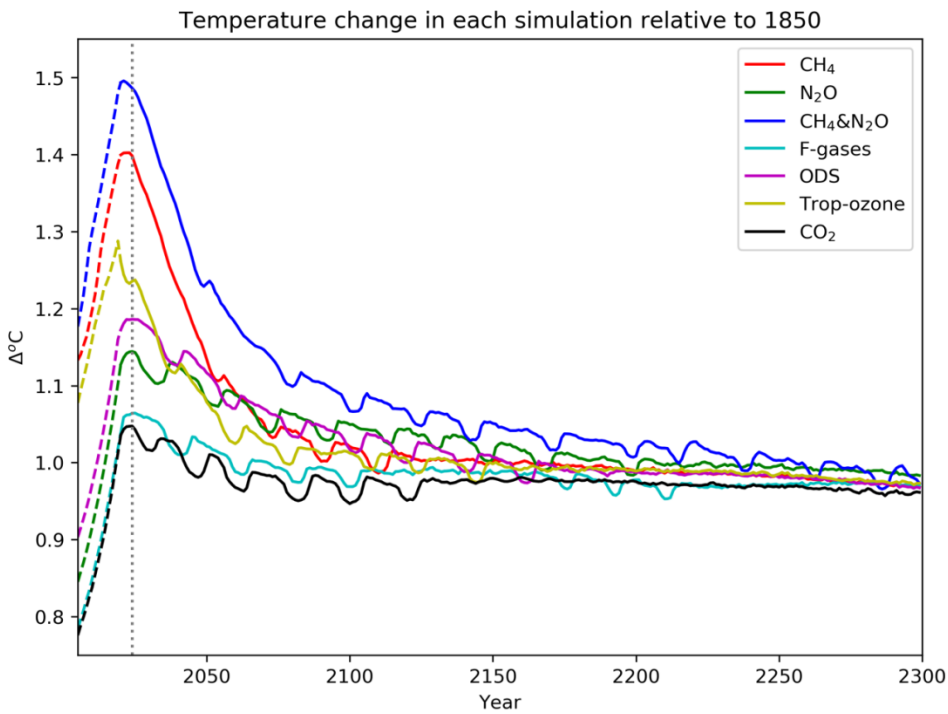

Figure 5.4: Present-day and future SAT change following zeroed emissions per individual or groups of non-CO_2 GHGs and CO_2. Solid lines represent the change in SAT after zero emissions and dashed lines represent the present-day (2005-2019) temperature change. By 2300, all simulations (with the exception of the CH_4& N_2O simulation converge on the temperature of the CO_2 simulation.

Figures 5.4 and 5.5 demonstrate the peak temperature change and reversibility of that increase in each scenario (including CO_2) from two different angles. In Figure 5.4 peak

temperature change is shown relative to 1850, with the dashed vertical line representing the year in which temperatures peak during the CO_2 only simulation. Because aerosols, which constitute a net cooling effect, are excluded in these simulations, peak temperature changes are higher in Figure 5.4 than has actually occurred. In all non-CO_2 GHG simulations, except F-gases, emissions prior to 2019 (dashed coloured lines) result in an increase in temperature compared to the CO_2 only simulation. Following zero emissions, temperature change in all simulations converges on the temperature change in the CO_2 only simulation. As CO_2 is included in the non-CO_2 GHG simulations, this shows that long-term temperature change is driven primarily by CO_2.

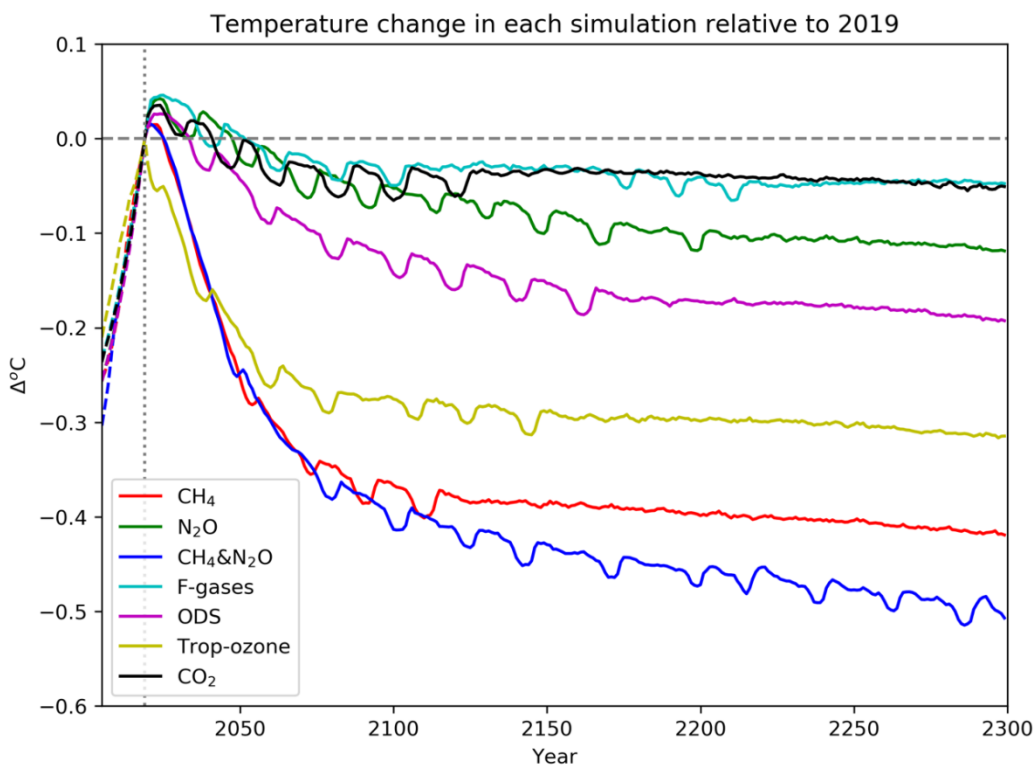

Figure 5.5: Trajectory of the change in SAT after zeroed emissions per individual or groups of GHGs. Change in SAT is relative to the change in SAT value for each simulation at the time of ZEC (grey dotted line). The horizontal grey dashed line represents the temperature in the CO_2 only simulation at the time of ZEC if that temperature were taken zero. This figure emphasizes the marginal cooling from F-gases (teal line) and N_2O (green line), and shows the more immediate effect of zeroing CH_4 (red and blue lines).

However, Figure 5.5 shows that the historical temperature change caused by individual and most groupings of non-CO_2 GHGs, can be reversed. Negative values here indicate a cooling post ZEC and reveal the reversibility of the peak temperature shown in Figure 5.4. Simulations with

higher historical warming exhibit the greatest reversibility. As well, simulations that include CH_4 display the most rapid temperature reversibility, seen by the steep decline in temperature after zero emissions. The simulation forced by N_2O alone, however, yields less cooling and therefore the reversibility of temperature changes caused by historical N_2O emissions is less than that for historical CH_4 emissions. Relative to 2019, the simulation forced by tropospheric ozone appears to yield a reduced rate of cooling compared to the cooling shown from trop-ozone alone in Figure 5.3. This happens because the results shown in Figure 5.5 include forcing from CO_2, which means the more tropospheric ozone forcing declines, the greater the influence of CO_2 on temperature change. Therefore when temperature change stabilize in the trop-ozone simulation shown in Figure 5.5, it remains higher than for the CO_2-only simulation.

Table 5.3: Percent of peak temperature change remaining from historical emissions of individual and non-CO_2 GHGs groupings. In each calculate a 20-year average of percent peak temperature change remaining (see, Eq. 5.1) was taken centered on the year indicated. *: the 108% of peak temperature change remaining for N_2O centered at 2050 is not accurate. This erroneous value is the result the climate variability described in Chapter 6.1. Due to internal climate variability (see Figure 5.3), the results in 2200 and 2290 for F-gases negligible.

Percent peak temperature change remaining after ZEC per individual and non-CO_2 GHG groupings				
	Year			
Gases	2050	2100	2200	2290
CH_4	44.9	14.0	6.4	4.7
N_2O	108.2*	79.6	26.0	28.0
CH_4 & N_2O	56.5	27.8	12.0	6.2
F-gases	130.2	100.8	-	-
ODS	83.9	45.5	8.1	5.6
Trop-ozone	12.9	6.6	3.4	3.0

Considering historical temperature reversibility as a percentage of peak temperature change remaining (see Chapter 5.3 Eq. 5.1), non-CO_2 GHGs exhibits a range of lingering effects on temperature change over the long-term timescale. Table 5.3 shows the percent of peak temperature change remaining per gas or gas grouping centered on specific years. Over the decadal period following zeroed emissions (2050), most gases yield over 40% peak temperature change remaining and tropospheric ozone yields 12.9% peak temperature change remaining. This suggests that a

portion of the temperature change caused by non-CO_2 GHG emissions prior to ambitious downscaling, expect for trop-ozone, remains in the atmosphere in the decades immediately following mitigation. Though that portion is highest for the F-gases, the aggregated ERF for F-gases is marginal and thus the higher percentage of peak temperature change remaining after ZEC for F-gases is mostly the result of a low denominator in Eq 5.1. The major gas N_2O, however, has a high ERF and century-scale lifetime, leading to approximately 80% of the peak temperature change caused by historical N_2O emissions to remain during this century (2100). At the century scale over 90% of the peak temperature change caused by historical CH_4 and ODSs have been removed from the atmosphere, therefore showing that over long periods this peak temperature change can almost entirely be reversed.

5.3.3 Historical and long-term ocean temperature and carbon cycle changes

Despite the reversibility of the historical and peak temperature change caused by past CH_4, ODS emissions and tropospheric-ozone precursor emissions, over the century timescale, there are additional consequences from past emissions on the climate system. In Figure 5.6, I show the influence of historical non-CO_2 emissions on average ocean temperature change over the long-term following zero emissions. Where historical emissions from CH_4, CH_4& N_2O, and tropospheric-ozone lead to higher historical warming (see Figure 5.3), there is a resultant increase in historical average ocean temperature. Meanwhile, in the decades following zeroed emissions, simulations driven by gases with short atmospheric lifetimes, show a steep decline in ocean heat flux (radiative forcing from the atmosphere to the ocean). Due to the high heat capacity of the ocean, however, it can take on this radiative forcing (heat) and gradually retain it as a change in average temperature over long timescales.

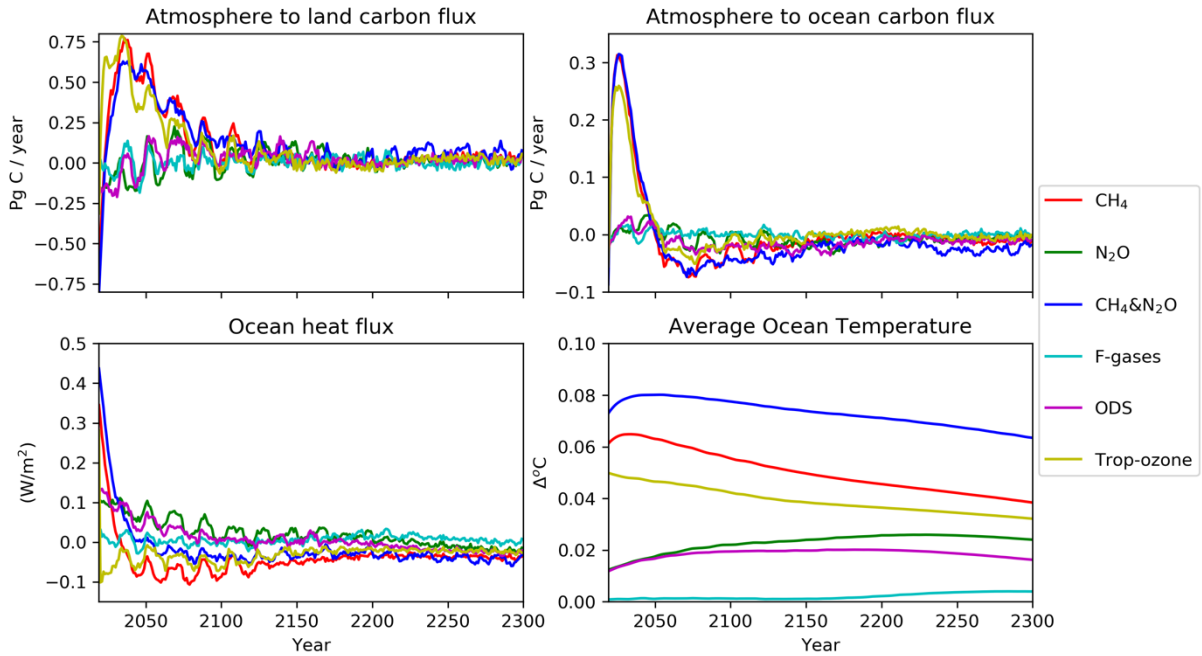

Figure 5.6: Carbon and heat fluxes and average ocean temperature change from time of ZEC to 2300. Each gas or gas grouping is shown relative to CO_2. Geophysically, past emissions from non-CO_2 GHGs do and will not significantly alter select components of the carbon cycle. The flux of carbon from the atmosphere to land (surface and vegetation) remains minimally higher under scenarios with higher peak temperature, than for CO_2, but equilibrates by approximately 2100. Only for average ocean temperature change (a proxy for sea-level rise) are differences notable. Despite a warming reversibility, scenarios with CH_4 lead to the highest levels of ocean temperature continuing out to 2300. From the historical warming caused by CH_4 alone (red lines), over a 0.06 °C increase in average ocean temperature is expected relative to CO_2 alone.

For past emissions from CH_4 and CH_4 & N_2O together, the fast decline in ocean heat flux is followed by a small initial increase in average ocean temperature. For other gases with a more stable ocean heat flux, average ocean temperature more gradually rises over for multiple centuries following zero emissions. Across the range gases studied here, the commitment of average ocean temperature change from past non-CO_2 GHG emissions varies between a cooling of 0.02 to a warming of 0.01 ºC, and in all cases, ocean temperature change at the point of zeroed emissions was higher than for CO_2 alone. As a result, any average ocean temperature change caused by historical or future non-CO_2 GHG emissions will persist for multiple centuries after emissions cease.

The impact of past non-CO_2 GHG emissions on atmosphere to land and ocean carbon fluxes is minimal over the long-term. By the end of this century, 80 years after ZEC, the carbon

fluxes from all individual gases and gas groupings fluctuate around 0 Pg C/year, indicating the establishment of an equilibrium between carbon pools at that timescale. In the decades after zero emissions, a small short-lived increase in atmosphere to land and ocean carbon flux is shown for simulations with rapid cooling. This increase in the atmosphere to land and ocean carbon fluxes occurs as a response of the land and ocean carbon pools to cooling, which strengthens the carbon pools until an approximate equilibrium between the atmosphere and land and ocean carbon pools is reached.

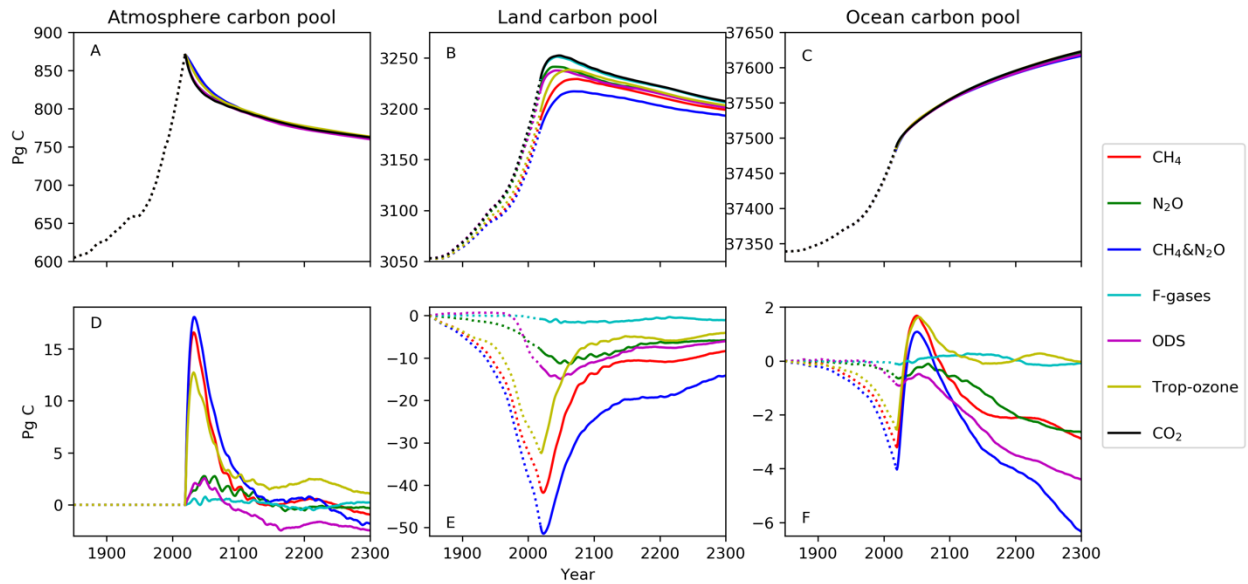

*Figure 5.7: Atmosphere, land, and ocean carbon pools. Plots A-C show the evolution of the total carbon pool in each simulation including CO_2. Plots D-F show the same evolution but for individual and groupings of non-CO_2 GHGs relative to CO_2. Dotted lines show the historical (1850-2019) evolution of the carbon pools and solid lines represent the carbon pools after zeroed emissions. *: over the historic period in plot D the atmosphere is shown to have a stable carbon pool. This occurs because in all simulations CO_2 concentration was prescribed over the historic period, therefore the atmosphere carbon pool was not able to evolve naturally.*

Figure 5.7 plots A and B show that changes to the atmosphere and land carbon pools are mostly driven by historical CO_2. As a result of past temperature change from individual and groupings of non-CO_2 GHGs, there is a slight decrease in the land carbon pool (Figure 5.7, plot E). This suggests that as historical temperature increases, the land exhibits a reduced capacity to uptake carbon from the atmosphere. To a nearly linear approximation (see Figure 5.8), for every 0.1 ^{o}C of past temperature increase attributable to non-CO_2 GHGs, there is a 10 Pg C reduction in

the land carbon pool. Compared to changes in the total land carbon pool, however, the decrease to the land carbon pool caused by historical non-CO_2 GHGs is minimal.

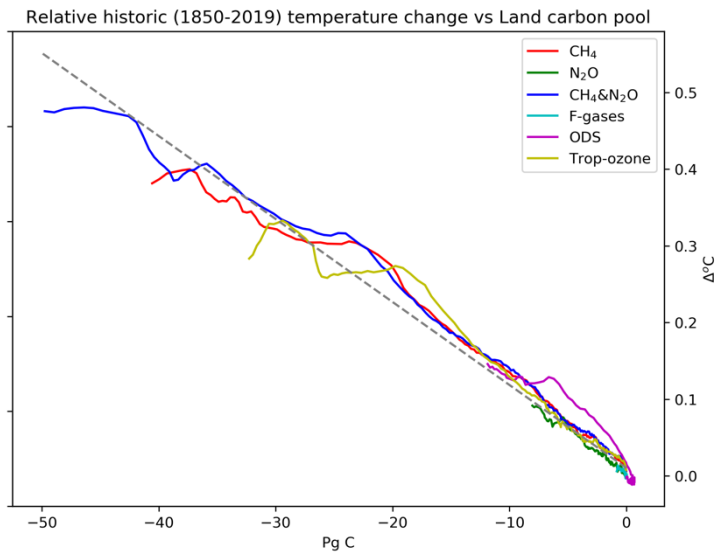

Figure 5.8: Historical temperature change per individual and groupings of non-CO_2 GHGs against the historical evolution of the land carbon pool per individual and groupings of non-CO_2 GHGs. This represents Figure 5.3 on the y-axis and Figure 57, plot E on the x-axis. The grey dashed line is the linear regression across all simulations, where $R^2 = 0.98$.

To a lesser increment, the atmosphere to ocean carbon flux and ocean carbon pool are impacted by past non-CO_2 GHG temperature change. Where non-CO_2 GHG induced temperature change increases over the historical period, a small reduction in the ocean carbon pool is observed (Figure 5.7, plot F). For the scenarios forced by CH_4, during the first two decades after zero emissions the ocean absorbs carbon from atmosphere at an increased rate, then returns to the baseline (Figure 5.6).

5.3.4 Fossil fuel and land use change

Considering that CO_2 and non-CO_2 GHGs typically share a common emissions source (Rogelj et al., 2014; Rogelj et al., 2015; Mengis & Matthews, 2019), it is possible to use similar non-CO_2 GHG disaggregation as above to assess how temperature changes in the absence of

greenhouse gas emissions from a specific source. The two main sources of GHG emissions are fossil fuel combustion (FFC) and land use change and agriculture (LUC).

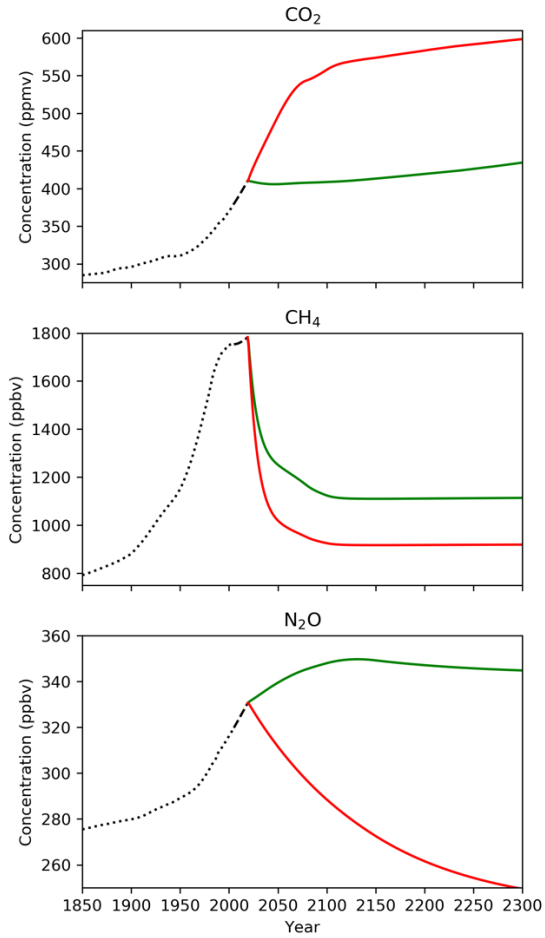

Figure 5.9: Atmospheric concentration of CO_2, CH_4, and N_2O under historic-to-near-present and RCP4.5 scenarios. Red solid lines represent FFC and other anthropogenic emissions continuing under RCP4.5 and LUC emissions stopping at year 2020. Green solid lines show LUC and other anthropogenic emissions continuing under RCP4.5 and FFC emissions stopping at year 2020.

In figure 5.9 I examine the progression of concentration for the main GHG's included in these scenarios – CO_2, CH_4, and N_2O. Due to the positive feedback between the land carbon pool, increasing temperature change, and the atmospheric carbon pool (see Chapter 5.3.3), and to a high portion of CO_2 emissions from FFC sources, CO_2 concentration rapidly increases over the 21st century and continues increasing over the long-term during the continuation of FFC and other anthropogenic emissions and zeroing of LUC emissions. Under either scenario the concentration

of methane rapidly decreases after 2020. This is, again, the result of the short atmospheric lifetime of CH_4, where here the atmospheric sink of CH_4 removes CH_4 at a greater rate than emissions are adding to it. For N_2O concentrations, only when LUC emissions are stopped and FFC and other anthropogenic emissions continue does the sink outweigh the source. Whereas when FFC emissions are stopped and LUC and other anthropogenic emissions continue, the source of N_2O to the atmosphere is only diminished by 30% (see Table 5.1) and the concentration of N_2O continues grow in that scenario.

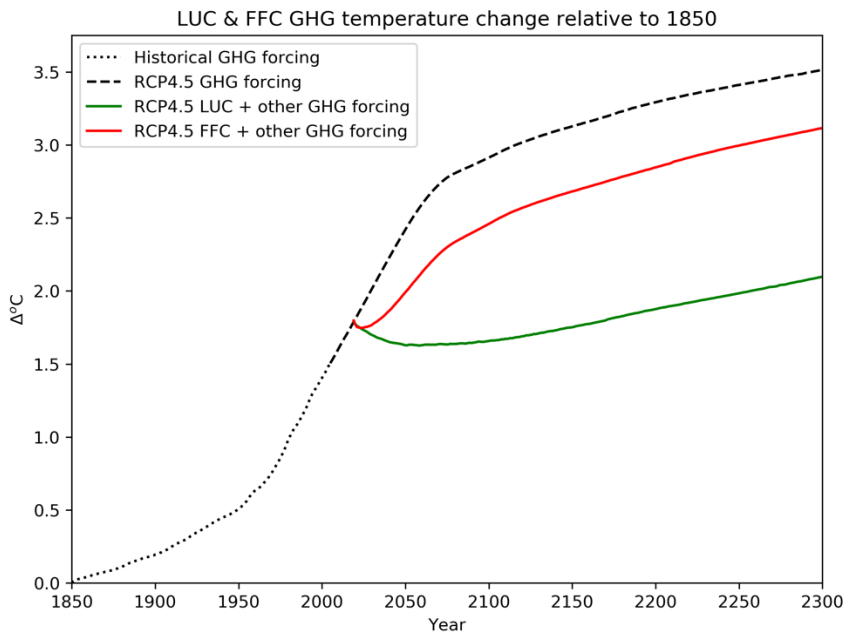

Figure 5.10: Land-use change and agriculture (LUC-green) and fossil fuel carbon (FFC-red) projected temperature change from greenhouse gases only. Both red and green lines include other anthropogenic emissions. Temperature is shown relative to 1850. Near-present (2005-2019) and projected temperature change from RCP4.5 forcing including CO_2, CH_4, N_2O, and tropospheric ozone is represented by the dashed line. From 2020, the FFC simulation includes RCP4.5 forcing scaled to FFC and other anthropogenic emissions. From 2020, the LUC simulation include RCP4.5 forcing scaled to LUC and other anthropogenic emissions.

Temperature change after zeroing GHG emissions from each source, while maintaining emissions from all other sectors (see Table 5.1), is demonstrated in Figure 5.10. To keep consistency with the above work these scenarios do not include emissions from aerosols and therefore the temperature change shown here should be viewed as artificially high.

Results from Figure 5.10 show a positive multi-century temperature change for both FFC and LUC emissions. This happens because under both scenarios, CO_2 emissions continue, if at a reduced rate, and because of the positive feedback between increasing temperature and increasing CO_2 concentration. Over the decade following zero FFC GHG emissions (green line), LUC and other anthropogenic GHG emissions lead to a small decline in temperature followed by increasing temperature over the century timescale. On the other hand, temperature briefly declines following zero LUC GHG emissions and continued FFC and other anthropogenic GHG emissions. Here continued FFC and other anthropogenic GHG emissions lead to approximately 1.3 ºC warming relative to 2020, when LUC GHG emissions are stopped.

Table 5.4: Temperature change avoided by cessation of emissions from a given source, assuming all other GHG emissions continue. Calculation is made as the difference between the dashed line (RCP4.5 GHG-only projected forcing), and solid lines in the listed years. 'Red' indicates LUC GHG emissions are set to zero and FFC and other anthropogenic GHG emissions continue under RCP4.5. 'Green' indicates FFC GHG emissions are set to zero and LUC and other anthropogenic GHG emissions continue under RCP4.5.

Temperature avoided by cessation of emissions per source				
	Year			
Simulation	2050	2100	2200	2290
LUC (red)	0.44	0.46	0.45	0.41
FFC (green)	0.8	1.2	1.4	1.4

Again, as aerosol emissions are not included in these simulations, these temperature increases post 2020 are unrealistically high. A more relevant metric is the temperature change avoided by cessation of emissions from one sector. Table 5.4 displays this avoided temperature change at four intervals over long-term timescale. Stopping GHG emissions from LUC activities yields between 0.41-0.46 ºC temperature avoided. Over the century timescale that temperature change avoided is 10-fold higher if FFC emissions are set to zero and LUC and other anthropogenic emissions continue.

5.4 Discussion

Over long-term periods following the idealized scenario in which greenhouse gas emissions stop, or the zero emissions commitment scenario, past emissions from individual and groupings of non-CO_2 GHGs do not lead to 1.5 ºC temperature change. This follows a similar conclusion from Smith et al. (2019). Though their study focused on the concept of future emissions commitment resultant from existing fossil fuel infrastructure, they also analyzed the ZEC from CO_2, aggregated non-CO_2 GHGs, and aerosols. From modelling the historical forcing of these three pollutants and ceasing emissions in 2018, an end of century (2100) cooling of 0.2 ºC was reported. Likewise for all pollutants, Matthews & Zickfeld (2012) calculated warming commitment in 2200 of approximately 0.1 °C, after zero emissions in 2010.The main difference between my scenarios and those of Matthews & Zickfeld (2012) and Smith et al. (2019) are that I excluded human induced negative forcers from the scenarios. In their experiments where all emissions are zeroed, the aerosol concentration in the atmosphere drops to near zero within the first few years after ZEC, leading to an initial warming followed by cooling converging on the warming commitment from CO_2. On the century timescale looked at here, the aerosol effect on warming commitment would have quickly dispersed from the atmosphere.

Studying the effect of non-CO_2 GHGs (namely, CH_4) on thermal expansion of the ocean, Zickfeld et al. (2017) used a similar ZEC scenario where they forced the UVic-ESCM with historical and projected emissions to 2050, 2100, and 2150 under RCP8.5 before setting emissions to zero. Our results are similar with respect to the how the ocean is effected by past non-CO_2 GHG emissions. We both show that the amount of average ocean temperature change and thus thermal sea-level rise are dependent on the level of atmospheric temperature change (i.e. emissions) prior to emissions abatement. Where Zickfeld et al. (2017) focus on how stopping CH_4 emissions after different levels of historical forcing will impact thermal sea-level rise, I extend their analysis to

include the remaining non-CO_2 GHGs. For non-CO_2 GHGs other than CH_4 and tropospheric ozone, historical emissions from gases with longer lifetimes such as N_2O result in continued ocean warming over the coming centuries. There is therefore an increased risk for the ocean from climate change resultant from longer-lived non-CO_2 GHGs.

Though my analysis shows emissions from non-CO_2 GHGs will augment the peak temperature caused by CO_2 emissions and lead to a minor cooling or warming of average ocean temperature following zero emissions, the impact on atmospheric temperature is not permanent. This observation echoes the argument of Bowerman et al. (2013), who showed that the effect on peak temperature of short-lived GHGs dissipates after emissions from those gases are reduced. Under a 20-year shorter analysis and zeroing emissions after much less historical temperature increase, my results of peak temperature change remaining are consistent with Zickfeld et al. (2017), who reported approximately the same percentage of peak warming remaining for CH_4, N_2O, and ODSs. Due to the relatively short lifetime of the strongest non-CO_2 GHG, CH_4, over half of the peak temperature exerted by past emissions is removed from the atmosphere within three decades and its historic signal continues as a minor contributor to future warming. As such, the influence of methane mitigation on long-term temperature change is maximized when coupled with CO_2 mitigation. Because under ZEC scenarios, mitigating methane leads to a return to temperature change driven by cumulative CO_2 emissions within this century, there is little additional advantage for atmospheric temperature change to policies favouring mitigation of methane in place of CO_2.

This argument counters that of a recent study by Collins et al. (2018), who showed that methane mitigation can lead to increases in the carbon pools, which would yield to increased allowable carbon emissions (the remaining carbon budget) for ambitious targets to the year 2100.

Assessing how high versus low CH_4 mitigation scenarios drive changes in the carbon pools, Collins et al. (2018) found that for emissions trajectories leading to the 1.5 ^{o}C target, high methane mitigation results in a 33% increase in the land carbon pool compared to low methane mitigation. Under this scenario they showed that the land carbon pool would increase by approximately 75 Pg C by the end of the century (Collins et al., 2018). Whereas my results (Figure 5.6, plot E, red line) show a land carbon pool recovery of nearly 30 PgC over the same time period. There are two major difference between these figures: 1) my results of the land carbon pool recovery are preceded by a land carbon pool decline, where no such decline is explicitly stated in Collins et al.'s analysis, which should lead to a temperature increase feedback prior to methane mitigation; and 2) Collins et al. allow the evolution of emissions to yield temperatures that increase until the 1.5 ^{o}C threshold, thus meaning the land carbon pool recovers from a higher maximum temperature than my simulation with CH_4 only.

Using an atmospheric chemistry design similar to the module employed here, MacDougall & Knutti (2016) modelled the climate system responses as a result of constant emissions of a methane-like gas. They showed that emissions of non-CO_2 GHGs can cause climate system feedbacks that disrupt the carbon cycle, without interacting with the carbon cycle (MacDougall & Knutti, 2016). One such disruption is an increase in SAT followed by a return to baseline after zero emissions of the methane-like gas.

With respect to the atmosphere and ocean carbon pools, however, their results are not comparable here. The reason the results for the atmosphere carbon pool and ocean carbon pool of MacDougall & Knutti (2016) cannot be compared by my results is to do with the simulation methods I employed. In my simulations, between 1850 to 2019 the evolution of CO_2 concentration in the atmosphere was prescribed. This meant that the atmosphere carbon pool was not adjusted

by changes in the land carbon pool. As shown by MacDougall & Knutti (2016), increases in temperature from emissions that do not directly interact with the carbon cycle, should lead to a reduction in the land carbon pool and a related increase in the atmosphere carbon pool. However, in the simulations presented here, when non-CO_2 GHG emissions caused historical increases in temperature, that process was not able to occur. A consequence is that in my simulations, at the time of zeroed emissions (2020) the atmosphere carbon pool is not adjusted to historical changes in the climate system, which therefore leads to the sharp increases in the atmosphere and ocean carbon pool seen in Figure 5.7 plots D& F.

My results are, however, in line with the results from MacDougall & Knutti (2016) with respect to the land carbon pool. Where MacDougall & Knutti (2016) showed a decrease in the land carbon pool from temperature increases caused by a methane-like gas, I expand their analysis to show that that during periods of temperature increase caused by non-CO_2 GHGs, that relationship is approximately linear. Once non-CO_2 GHG emissions cease, however, this near-linearity does not hold. After zero emissions of individual and groupings of non-CO_2 GHGs, temperature change is driven by declining CO_2 concentrations, declining non-CO_2 GHG concentrations, and internal climate variability. Whereas, for this relationship, prior to emissions cessation, temperature change is driven by increasing concentration changes of non-CO_2 GHGs.

My analysis of the temperature change caused by source sectors follows highly idealized scenarios where all emissions from either FFC or LUC are zeroed at 2020. Compared to Smith et al. (2019), who found a 67% chance of exceeding 1.5 °C under a fast retirement scenario for fossil fuels, I find immediate cessation of FFC emissions could lead to an avoidance of 1.4 ºC temperature change compared to RCP4.5 GHG forcing. The difference between these calculations is that where Smith et al. (2019) include continued emissions from existing fossil fuel

infrastructure and assume differing rates of infrastructure retirement, my analysis assumes all fossil fuel combustion related emissions stop immediately.

That I exclude aerosols should not mean my results from stopping FFC emissions at 2020 and allowing LUC and other anthropogenic emissions to continue under RCP4.5 are invalid. Mengis & Matthews (2019) report that 97% of sulphate aerosol emissions are from FFC sources, which means almost all aerosols emissions would be stopped if they were included in this scenario. Temperature change would therefore follow a brief (less than a decade) period of warming with a return to the temperature change path seen in the green line in Figure 5.10 afterwards. Again, the effect of aerosols would be felt in the short period after 2020 and would be much less relevant to changes that occur on century timescales.

5.5 Conclusion

Minimal long-term temperature change and reversibility of peak warming from non-CO_2 GHGs agrees with the principle that CO_2 is the dominant constituent with respect to global warming. By the end of this century (2100), or extending out to 2300, temperature changes resulting from past individual and groupings of non-CO_2 GHGs emissions converges on the temperature change caused by past CO_2 emissions. Owing to the short atmospheric lifetime of CH_4 and tropospheric ozone, scenarios including past CH_4 emissions and forcing from tropospheric ozone show high reversibility of peak temperature change on century timescales.

My results suggest that if FFC GHG emissions are brought to zero, approximately 1.4 ºC of global warming can be avoided, relative to a scenario of moderate mitigation effort as is the case of RCP4.5. This implies that there is some room for GHG emissions from LUC and other

anthropogenic activities, including agricultural practices, to continue under deep mitigation scenarios and ambitious climate target scenarios.

CHAPTER 6

EXPANDED DISCUSSION &CONCLUSIONS

6.1 Climate system response variability

In my experiments there is variability in temperature change following emissions cessation. Though the trend of declining temperature post-2020 is more important than the decadal variability seen in Figures 5.2-5, that variability could attribute to an increased uncertainty in my results regarding the reversibility of peak temperature, especially with respect to N_2O. As such, I will address a possible cause of these fluctuations here. To focus the discussion, I'm showcasing results from the CH_4& N_2O simulation, without making results relative to CO_2 – i.e. CO_2 forcing following zero emissions is here included. This simulation is showcased because it yielded the highest peak warming and the variability in temperature change continues over the century scale, whereas in the remaining simulations temperature change stabilizes after 2200 (see Figure 5.2 and 5.5).

Figure 6.1 shows the evolution of sea ice, surface albedo, and average surface air temperature (SAT) in the Northern hemisphere following zero emissions. Prior to 2020 (dashed lines), the climate system was in a state of increasing forcing, Subsequently, global sea ice area and Northern hemisphere sea ice area were in states of decline. After 2020, however, the climate system entered a state of cooling or recovery. In this century (up to 2100), peak temperature rapidly declines due to the short lifetime of CH_4 and only minor fluctuations in global sea ice area and hemispheric sea ice area are observed. As the legacy on peak temperature of historical N_2O and CO_2 forcing continues to drive temperature beyond 2100, global sea ice area exhibits increased decadal or bi-centennial variability. Those changes are localized to the Northern hemisphere (Southern hemisphere sea ice area is approximately stable over this period).

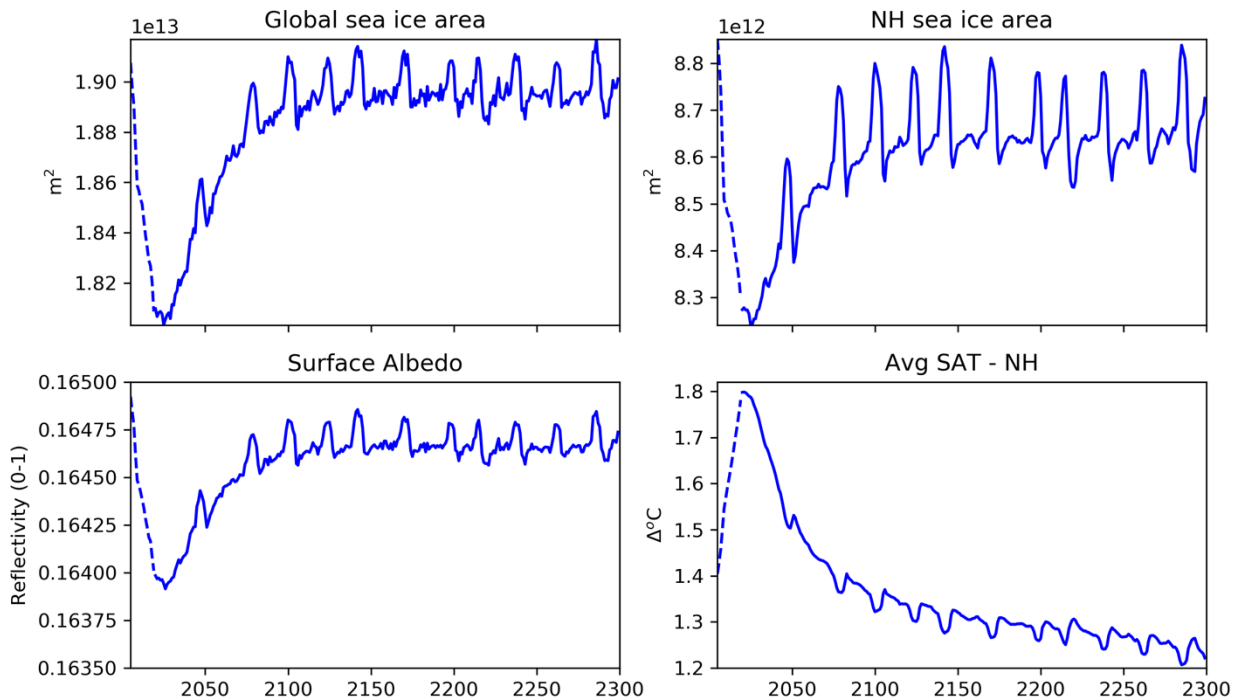

Figure 6.1: Sea ice area, global surface albedo and the change in average surface air temperature in the Northern hemisphere relative to 1850 for the simulation forced by CH_4, N_2O, and CO_2 from 1850 to 2019. Dashed lines represent forcing from CH_4 and N_2O emissions between 2005 to 2019, while CO_2 concentration was prescribed. Solid lines represent forcing following zero emissions from all three forcers.

The effect of increasing and decreasing sea ice area is to oscillate the amount of planetary surface area that is highly reflective to incoming solar radiation. This translates to short-lived increases in the planetary surface albedo, which decreases the quantity of incoming solar radiation that warms surfaces (ocean and land). Despite the minor magnitude of these short-lived increases in global surface albedo, they cause short-lived decreases in SAT, which is again localized to the Northern hemisphere.

The driver of fluctuating Northern hemisphere sea ice area is unknown. One answer could be that ocean circulation or average temperature are unstable following rapid temperature decline. However, as seen in Figure 5.6, average ocean temperature change is stable over the long-term, therefore ocean changes should not cause sea ice area growth and retreat. From a modelling perspective, an explanation could be that simulations were started with the climate not in

equilibrium. At the time simulations were run, there was little evidence to support this latter conclusion, but it remains possible. The most likely answer is that, due to ongoing updates within components of the UVic-ESCM that my module does not directly interact with, there is drift in the model version I used to run these simulations. As evidence, the CO_2 simulation includes no forcing from updates I made, yet in the first century following zero CO_2 emissions, a similar variability in SAT is observed (see Figure 5.4).

Where this variability in temperature change post-2020 in the CO_2 simulation does not align with the variability in temperature change in the non-CO_2 GHG simulations post-2020, that fluctuation is exasperated per individual or groupings of non-CO_2 GHGs. This interdependence on temperature change is responsible for the high variability in temperature change from N_2O relative to CO_2 following zero emissions seen in Figure 5.3. That high variability is what caused an average 108% of peak temperature change to be remaining from historical forcing from N_2O after zero emissions. Despite the high variability in temperature change after emissions stop for N_2O and the remaining non-CO_2 GHGs, the trend of temperature decline is not irrecoverably disturbed. Therefore, these fluctuations in temperature change post-2020 do not cause a strong enough disturbance in the climate system to discount my results.

6.2 Conclusions

Global warming represents one of the greatest challenges in human history. To combat this problem which our activities has produced, we are seeking to keep global temperature from exceeding 1.5 ^{o}C above pre-industrial levels (UNFCCC, 2015). Most of this global warming has already occurred and is primarily the result of cumulative carbon dioxide emissions (Matthews & Solomon, 2013). This historical warming caused by historical cumulative CO_2emissions has been

previously shown to persist for hundreds of years regardless of future emissions (Solomon et al., 2009; Matthews & Zickfeld, 2012; Allen et al., 2018b).Past emissions from CO_2 and other greenhouse gases can further cause lasting climatological impacts such as sea-level rise (Ehlert & Zickfeld, 2017; Zickfeld et al., 2017). Here I investigated the addition of non-CO_2 greenhouse gases into this temperature regime and quantified how their historical forcing effected temperature in the absence of future GHG emissions.

My analysis made use of the idealized Zero Emissions Commitment scenario where, following a spin-up of historical forcing, GHG emissions from CO_2 and individual and policy relevant groupings of non-CO_2 GHGs were assumed to abruptly stop (Solomon et al., 2009; Matthews & Zickfeld, 2012). By then allowing the concentrations of CO_2 and non-CO_2 GHGs to evolve based on model results, I was able to quantify the percent of peak temperature change that can be reversed over decadal and century timescales. I showed that for non-CO_2 GHGs with short lifetimes (namely methane and tropospheric ozone), more than half of the peak temperature change their historical emissions cause can be reversed within three decades of zero emissions. For gases with longer lifetimes, such as nitrous oxide, I showed that nearly 80% of the peak temperature change from historical emissions will persist until the end of this century, whereas only 30% will persist by the end of the next century (2200).

Because global surface air temperature change is not the only important measure of global warming, I extended my analysis to assess how historical non-CO_2 GHG forcing effected and will affect carbon fluxes, carbon pools, and the average ocean temperature change. I calculated that past temperature change resultant from non-CO_2 GHG emissions could individually and in groupings have led to between 0 – 0.08 ºC increase in average ocean temperature. This increase could already have consequences for sea-level rise resultant from thermal expansion of the ocean,

which is an impact of ocean temperature increase. I have showed average ocean temperature will remain approximately constant or increase for multiple centuries after zero emissions depending on the lifetime of the gas in question. I further confirmed that increases in temperature from past non-CO_2 GHG emissions will lead to reductions in the land carbon pool, that should (though not proven here) lead to a feedback on the atmosphere carbon pool.

Considering the warming reversibility and climate impacts from specific and groupings of non-CO_2 GHGs does not account for the fact that GHG emissions often share the same source. To explore the effect of co-emitted gases, I included simulations where I partitioned emissions from CO_2, CH_4, N_2O, and tropospheric-ozone by their source to quantify the amount of warming that could be avoided if one source sector was to stop emissions immediately. With these simulations I demonstrated that eliminating land-use change and agriculture emissions (an impractical scenario at best) while continuing fossil fuel combustion and other anthropogenic emissions would lead to approximately 0.45 ^{o}C of avoided warming over multiple centuries, relative to continued emissions from all other sectors following RCP4.5. In the same scenario, eliminating fossil fuel combustion while continuing activities from land use change and agriculture and other sectors could lead to approximate 1.4 ^{o}C of avoided warming over multiple centuries.

My analysis covered temperature and climate change from greenhouse gases only. As such a key component of the radiative balance of the climate system was missing – aerosols. Emissions of aerosols cause a reduction in the net planetary radiative forcing and thus a reduction in temperature change (Myhre et al., 2013). Therefore, the total historical warming exhibited in my scenarios is artificially inflated. With respect to the by-source scenarios, there is a need for future work to include aerosol emissions.

Furthermore, the by-source scenarios and analysis could benefit from expanding to include emissions projections from the remaining RCP scenarios as well as the more recent Shared Socio-economic Pathway scenarios. Simulating these additional emissions paths would yield a range of plausible storylines for warming avoidance by removing emissions from one sector. This expansion of my work would help to better define the uncertainty of warming avoidance, as well as provide a more robust account of baselines for deep mitigation policies.

Despite these limitations, my study contributes to the literature in this area by defining the percentage of peak warming that can be reversed by mitigating non-CO_2 GHGs, which should be understood as a maximum warming reversibility. This builds off the knowledge that non-CO_2 GHGs can augment peak temperature change caused by CO_2 before deep mitigation takes place and that deep mitigation of non-CO_2 GHGs, coupled to CO_2 mitigation will lead to a short period of global cooling (Matthews & Zickfeld, 2012; Bowerman et al., 2013;Zickfeld et al., 2017; Allen et al., 2018b). Another advance my study made was to quantify the relationship between warming from historical non-CO_2 GHGs and reductions in the land carbon pool, which appears to be approximately linear over the temperature changes considered here.

From my results, it is evident that combined mitigation of non-CO_2 GHGs and CO_2 will have positive (i.e. global cooling) decadal and longer-term effects on the climate system. However, non-CO_2 GHG mitigation in the absence of CO_2 mitigation is not here shown to be an effective method for reversing warming over long timescales. My results further indicate that with aggressive downscaling of fossil fuel combustion emissions, it is possible within the emissions framework studied here, to continue activities from land-use change and agriculture and potentially remain in line with ambitious climate targets.

REFERENCES

Allen, M. R., Frame, D. J., Huntingford, C., Jones, C. D., Lowe, J. A., Meinshausen, M., & Meinshausen, N. (2009). Warming caused by cumulative carbon emissions towards the trillionth tonne. *Nature, 458*(7242), 1163-1166. doi:10.1038/nature08019

Allen, M. R., & Stocker, T. F. (2014). Impact of delay in reducing carbon dioxide emissions. *Nature Climate Change, 4*(1), 23-26. doi:10.1038/NCLIMATE2077

Allen, M. R., Fuglestvedt, J. S., Shine, K. P., Reisinger, A., Pierrehumbert, R. T., & Forster, P. M. (2016). New use of global warming potentials to compare cumulative and short-lived climate pollutants. *Nature Climate Change, 6*(8), 773-+. doi:10.1038/NCLIMATE2998

Allen, M. R., Shine, K. P., Fuglestvedt, J. S., Millar, R. J., Cain, M., Frame, D. J., & Macey, A. H. (2018a). A solution to the misrepresentations of CO2-equivalent emissions of short-lived climate pollutants under ambitious mitigation. *Npj Climate and Atmospheric Science, 1*, 16. doi:10.1038/s41612-018-0026-8

Allen, M., Babiker, M., Chen, Y., de Coninck, H., Connors, S., van Diemen, R., … Zickfeld, K. (2018b). IPCC, 2018: Summary for Policymakers. In: *Global warming of 1.5 °C. An IPCC Special Report on the impacts of global warming of 1.5 °C above pre-industrial levels and related global greenhouse gas emission pathways, in the context of strengthening the global response to the threat of climate change, sustainable development, and efforts to eradicate poverty.* [Masson-Delmotte, V., Zhai, P., Portner, H. O., Roberts, D., Skea, J., Shukla, P. R., … Waterfield, T. (eds)]. World Meteorological Organization, Geneva, Switzerland.

Bowerman, N. H. A., Frame, D. J., Huntingford, C., Lowe, J. A., Smith, S. M., & Allen, M. R. (2013). The role of short-lived climate pollutants in meeting temperature goals.*Nature Climate Change, 3*(12), 1021-1024. doi:10.1038/NCLIMATE2034

Ciais, P., Sabine, C., Bala, G., Bopp, L., Brovkin, V., Canadell, J., … Thornton, P. (2013). Carbon and other biogeochemical cycles. In: *Climate change 2013: The physical science basis. Contribution to working group I to the Fifth Assessment Report of the International Panel on Climate Change*. [Heinze, C., Tans, P., &Vesala, T. (eds)]. Cambridge University Press, Cambridge, United Kingdom and New York, NY, USA.

Collins, W.J., Webber, C.P., Cox, P.M., Huntingford, C., Lowe, J., Sitch, S., Chadburn, S.E., Comyn-Platt, E., Harper, A.B., Hayman, G., Powell, T. (2018). *Environmental Research Letters*, *13*(3), 054003. doi:10.1088/1748-9326/aab89c

Eby, M., Zickfeld, K., Montenegro, A., Archer, D., Meissner, K. J., & Weaver, A. J. (2009). Lifetime of anthropogenic climate change: Millennial time scales of potential CO2 and surface temperature perturbations. *Journal of Climate, 22*(10), 2501-2511. doi:10.1175/2008JCLI2554.1

Ehalt, D., Prather, M., Dentener, F., Derwent, R., Dlugokencky, E., Holland, E., … Wang, M. (2001). Atmospheric chemistry and greenhouse gases. In: *Climate change 2001: The physical science basis. Contribution to working group I to the Third Assessment Report of the International Panel on Climate Change*. [Joos, F., & McFarland, M. (eds)]. Cambridge University Press, Cambridge, United Kingdom and New York, NY, USA.

Ehlert, D., &Zickfeld, K. (2017). What determines the warming commitment after cessation of CO2 emissions? *Environmental Research Letters, 12*(1), 015002. doi:10.1088/1748-9326/aa564a

Etminan, M., Myhre, G., Highwood, E. J., & Shine, K. P. (2016). Radiative forcing of carbon dioxide, methane, and nitrous oxide: A significant revision of the methane radiative forcing. *Geophysical Research Letters, 43*(24), 12614-12623. doi:10.1002/2016GL071930

Friedlingstein, P., Andrew, R. M., Rogelj, J., Peters, G. P., Canadell, J. G., Knutti, R., . . . Le Quere, C. (2014). Persistent growth of CO2 emissions and implications for reaching climate targets. *Nature Geoscience, 7*(10), 709-715. doi:10.1038/NGEO2248

Frölicher, T. L., Winton, M., & Sarmiento, J. L. (2014). Continued global warming after CO2 emissions stoppage.*Nature Climate Change, 4*(1), 40-44. doi:10.1038/NCLIMATE2060

Frölicher, T. L., & Paynter, D. J. (2015). Extending the relationship between global warming and cumulative carbon emissions to multi-millennial timescales. *Environmental Research Letters, 10*(7), 075002. doi:10.1088/1748-9326/10/7/075002

Gillett, N. P., Arora, V. K., Matthews, D., & Allen, M. R. (2013). Constraining the ratio of global warming to cumulative CO2 emissions using CMIP5 simulations. *Journal of Climate, 26*(18), 6844-6858. doi:10.1175/JCLI-D-12-00476.1

Hansen, J., Nazarenko, L., Ruedy, R., Sato, M., Willis, J., Del Genio, A., . . . Tausnev, N. (2005). Earth's energy imbalance: Confirmation and implications. *Science, 308*(5727), 1431-1435. doi:10.1126/science.1110252

Haustein, K., Allen, M. R., Forster, P. M., Otto, F. E. L., Mitchell, D. M., Matthews, H. D., & Frame, D. J. (2017). A real-time global warming index. *Scientific Reports, 7*, 15417. doi:10.1038/s41598-017-14828-5

Le Quéré, C., Andrew, R. M., Friedlingstein, P., Sitch, S., Hauck, J., Pongratz, J., . . . Zheng, B. (2018). Global carbon budget 2018. *Earth System Science Data, 10*(4), 2141-2194. doi:10.5194/essd-10-2141-2018

Levy, H., II. (1971). Normal atmosphere: Large radical and formaldehyde concentrations predicted. *Science, New Series,* 173.3992. 141-143.

MacDougall, A. H., & Friedlingstein, P. (2015). The origin and limits of the near proportionality between climate warming and cumulative CO2 emissions. *Journal of Climate, 28*(10), 4217-4230. doi:10.1175/JCLI-D-14-00036.1

MacDougall, A. H., Zickfeld, K., Knutti, R., & Matthews, H. D. (2015). Sensitivity of carbon budgets to permafrost carbon feedbacks and non-CO2 forcings. *Environmental Research Letters, 10*(12), 125003. doi:10.1088/1748-9326/10/12/125003

MacDougall, A. H., & Knutti, R. (2016). Enhancement of non-CO2 radiative forcing via intensified carbon cycle feedbacks. *Geophysical Research Letters, 43*(11), 5833-5840. doi:10.1002/2016GL068964

Matthews, H. D., Gillett, N. P., Stott, P. A., & Zickfeld, K. (2009). The proportionality of global warming to cumulative carbon emissions. *Nature, 459*(7248), 829-U3. doi:10.1038/nature08047

Matthews, H. D., & Zickfeld, K. (2012). Climate response to zeroed emissions of greenhouse gases and aerosols. *Nature Climate Change, 2*(5), 338-341. doi:10.1038/NCLIMATE1424

Matthews, H. D., & Solomon, S. (2013). Irreversible does not mean unavoidable. *Science, 340*(6131), 438-439. doi:10.1126/science.1236372

Matthews, H. D., Landry, J.-S., Partanen, A.-I., Allen, M., Eby, M., Forster, P. M., Friedlingstein, P., Zickfeld, K. (2017). Estimating carbon budgets for ambitious climate targets. *Current Climate Change Reports, 3,* 69-77. doi:10.1007/s4061-017-0055-0

Matthews, H. D., Zickfeld, K., Knutti, R., & Allen, M. R. (2018). Focus on cumulative emissions, global carbon budgets and the implications for climate mitigation targets. *Environmental Research Letters, 13*(1), 010201. doi:10.1088/1748-9326/aa98c9

Mauritsen, T., & Pincus, R. (2017). Committed warming inferred from observations. *Nature Climate Change, 7*(9), 652-+. doi:10.1038/NCLIMATE3357

Meinshausen, M., Smith, S. J., Calvin, K., Daniel, J. S., Kainuma, M. L. T., Lamarque, J., . . . van Vuuren, D. P. P. (2011b). The RCP greenhouse gas concentrations and their extensions from 1765 to 2300. *Climatic Change, 109*(1-2), 213-241. doi:10.1007/s10584-011-0156-z

Mengis, N., & Matthews, H. D. (2019). Non-CO_2 forcing changes will likely decrease the remaining carbon budget for 1.5 °C. *[submitted]*.

Mengis personal communication (2019)

Millar, R., Allen, M., Rogelj, J., & Friedlingstein, P. (2016). The cumulative carbon budget and its implications. *Oxford Review of Economic Policy, 32*(2), 323-342. doi:10.1093/oxrep/grw009

Millar, R. J., Fuglestvedt, J. S., Friedlingstein, P., Rogelj, J., Grubb, M. J., Matthews, H. D., . . . Allen, A. R. (2017). Emission budgets and pathways consistent with limiting warming to 1.5 degrees C. *Nature Geoscience, 10*(10), 741-+. doi:10.1038/NGEO3031

Myhre, G., Shindell, D., Breon, F.-M., Collins, W., Fuglestvedt, J., Huang, J., … Zhang, H. (2013). Anthropogenic and natural radiative forcing. In: *Climate change 2013: The physical science basis. Contribution to working group I to the Fifth Assessment Report of the International Panel on Climate Change*. [Stocker, T.F., Qin, D., Plattner, G.-K., Tignor, M., Allen, S.K., Boschung, J. … Midgley, P.M. (eds)]. Cambridge University Press, Cambridge, United Kingdom and New York, NY, USA.

Partanen, A., Leduc, M., & Matthews, H. D. (2017). Seasonal climate change patterns due to cumulative CO2 emissions. *Environmental Research Letters, 12*(7), 075002. doi:10.1088/1748-9326/aa6eb0

Pierrehumbert, R. T. (2014). Short-lived climate pollution. *Annual Review of Earth and Planetary Sciences, Vol 42, 42*, 341-+. doi:10.1146/annurev-earth-060313-054843

Riahi, K., van Vuuren, D. P., Kriegler, E., Edmonds, J., O'Neill, B. C., Fujimori, S., . . . Tavoni, M. (2017). The shared socioeconomic pathways and their energy, land use, and greenhouse gas emissions implications: An overview. *Global Environmental Change-Human and Policy Dimensions, 42*, 153-168. doi:10.1016/j.gloenvcha.2016.05.009

Ricke, K. L., & Caldeira, K. (2014). Maximum warming occurs about one decade after a carbon dioxide emission. *Environmental Research Letters, 9*(12), 124002. doi:10.1088/1748-9326/9/12/124002

Rogelj, J., McCollum, D. L., O'Neill, B. C., & Riahi, K. (2013). 2020 emissions levels required to limit warming to below 2 degrees C. *Nature Climate Change, 3*(4), 405-412. doi:10.1038/NCLIMATE1758

Rogelj, J., Schaeffer, M., Meinshausen, M., Shindell, D. T., Hare, W., Klimont, Z., . . . Schellnhuber, H. J. (2014). Disentangling the effects of CO2 and short-lived climate forcer mitigation. *Proceedings of the National Academy of Sciences of the United States of America, 111*(46), 16325-16330. doi:10.1073/pnas.1415631111

Rogelj, J., Meinshausen, M., Schaeffer, M., Knutti, R., & Riahi, K. (2015). Impact of short-lived non-CO2 mitigation on carbon budgets for stabilizing global warming. *Environmental Research Letters, 10*(7), 075001. doi:10.1088/1748-9326/10/7/075001

Saunois, M., Bousquet, P., Poulter, B., Peregon, A., Ciais, P., Canadell, J. G., . . . Zhu, Q. (2016). The global methane budget 2000-2012. *Earth System Science Data, 8*(2), 697-751. doi:10.5194/essd-8-697-2016

Seinfeld, J.H., & Pandis, S.P. (2016). *Atmospheric chemistry and physics: From air pollution to climate change, 3rd edition*. Hoboken, New Jersey: John Wiley & Sons Inc.

Shindell, D., Kuylenstierna, J. C. I., Vignati, E., van Dingenen, R., Amann, M., Klimont, Z., . . . Fowler, D. (2012). Simultaneously mitigating near-term climate change and improving human health and food security. *Science, 335*(6065), 183-189. doi:10.1126/science.1210026

Smith, S. M., Lowe, J. A., Bowerman, N. H. A., Gohar, L. K., Huntingford, C., & Allen, M. R. (2012). Equivalence of greenhouse-gas emissions for peak temperature limits. *Nature Climate Change, 2*(7), 535-538. doi:10.1038/NCLIMATE1496

Smith, C. J., Forster, P. M., Allen, M., Leach, N., Millar, R. J., Passerello, G. A., &Regayre, L. A. (2018). FAIR v1.3: A simple emissions-based impulse response and carbon cycle model. *Geoscientific Model Development, 11*(6), 2273-2297. doi:10.5194/gmd-11-2273-2018

Smith, C. J., Forstcr, P. M., Allen, M., Fuglestvedt, J., Millar, R. J., Rogelj, J., &Zickfeld, K. (2019). Current fossil fuel infrastructure does not yet commit us to 1.5 degrees C warming. *Nature Communications, 10*, 101. doi:10.1038/s41467-018-07999-w

Solomon, S., Plattner, G., Knutti, R., &Friedlingstein, P. (2009). Irreversible climate change due to carbon dioxide emissions. *Proceedings of the National Academy of Sciences of the United States of America, 106*(6), 1704-1709. doi:10.1073/pnas.0812721106

Tokarska, K. B., & Zickfeld, K. (2015). The effectiveness of net negative carbon dioxide emissions in reversing anthropogenic climate change. *Environmental Research Letters, 10*(9), 094013. doi:10.1088/1748-9326/10/9/094013

Tokarska, K. B., Gillett, N. P., Weaver, A. J., Arora, V. K., &Eby, M. (2016). The climate response to five trillion tonnes of carbon. *Nature Climate Change, 6*(9), 851-+. doi:10.1038/NCLIMATE3036

UNEP, (1987). Montreal Protocol on Substances that Deplete the Ozone Layer. 16 September 1987.Chapter XXVII. Montreal.

UNFCCC, (1998). Kyoto Protocol to the United Nations Framework Convention on Climate Change. (http://unfccc.int/sites/default/files/kpeng.pdf)

UNFCCC, C. (2015). Adoption of the paris agreement. I: Propos. by Pres. (Draft Decis. United Nations Off. Geneva (Switzerland)

van Vuuren, D. P., Edmonds, J., Kainuma, M., Riahi, K., Thomson, A., Hibbard, K., . . . Rose, S. K. (2011). The representative concentration pathways: An overview. *Climatic Change, 109*(1-2), 5-31. doi:10.1007/s10584-011-0148-z

Wania, R., Meissner, K. J., Eby, M., Arora, V. K., Ross, I., & Weaver, A. J. (2012). Carbon-nitrogen feedbacks in the UVic ESCM. *Geoscientific Model Development, 5*(5), 1137-1160. doi:10.5194/gmd-5-1137-2012

Weaver, A., Eby, M., Wiebe, E., Bitz, C., Duffy, P., Ewen, T., . . . Yoshimori, M. (2001). The UVic earth system climate model: Model description, climatology, and applications to past, present and future climates. *Atmosphere-Ocean, 39*(4), 361-428. doi:10.1080/07055900.2001.9649686

Williams, R. G., Roussenov, V., Frolicher, T. L., & Goodwin, P. (2017). Drivers of continued surface warming after cessation of carbon emissions. *Geophysical Research Letters, 44*(20), 10633-10642. doi:10.1002/2017GL075080

Zickfeld, K., Eby, M., Matthews, H. D., & Weaver, A. J. (2009). Setting cumulative emissions targets to reduce the risk of dangerous climate change. *Proceedings of the National Academy of Sciences of the United States of America, 106*(38), 16129-16134. doi:10.1073/pnas.0805800106

Zickfeld, K., Arora, V. K., & Gillett, N. P. (2012). Is the climate response to CO2 emissions path dependent? *Geophysical Research Letters, 39*, L05703. doi:10.1029/2011GL050205

Zickfeld, K., & Herrington, T. (2015). The time lag between a carbon dioxide emission and maximum warming increases with the size of the emission. *Environmental Research Letters, 10*(3), 031001. doi:10.1088/1748-9326/10/3/031001

Zickfeld, K., Solomon, S., & Gilford, D. M. (2017). Centuries of thermal sea-level rise due to anthropogenic emissions of short-lived greenhouse gases. *Proceedings of the National Academy of Sciences of the United States of America, 114*(4), 657-662. doi:10.1073/pnas.1612066114